

# Perturbation of the PET Process in Fluorophore–Spacer–Receptor Systems through Structural Modification: Transition Metal Induced Fluorescence Enhancement and Selectivity

Bamaprasad Bag and Parimal K. Bharadwaj\*

Chemistry Department, Indian Institute of Technology, Kanpur 208016, India

Received: June 7, 2004; In Final Form: January 12, 2005

Several fluorescent signaling systems are built in the format fluorophore–spacer–receptor with ethylenediamine or *N,N*-dimethylethylenediamine as the receptor, anthracene as the fluorophore, and a methylene group as the spacer. The receptors are derivatized with different electron-withdrawing groups such as 4-nitrobenzene, 4-nitro-2-pyridine, and 2,4-dinitrobenzene, to perturb the photoinduced intramolecular electron transfer (PET) process from the nitrogen lone-pair to the fluorophore. The photophysical properties of these supramolecular systems and their fluorescence responses toward a number of quenching transition metal ions are reported. It is shown that the PET is highly efficient in the absence of a metal ion. With a metal ion input, the fluorescence can be recovered to a different extent depending on the nature of the metal and on the overall architecture of the system as well. Despite the possibility of strong interaction between the fluorophore and the metal ion, significant fluorescence enhancement is observed with quenching of paramagnetic transition metal ions. The complex stability data show that the stability constants for the metal ions showing fluorescence enhancement are of the order of  $10^4 \text{ M}^{-1}$ . This study shows that structurally simple fluorescent signaling systems for quenching transition metal ions can be built by maximizing the PET. It is also shown here that simple structural modification can make these systems highly specific for particular transition metal ions for potential applications in several contemporary areas of research.

## 1. Introduction

Fluorescence signaling systems can be designed for signal transduction upon analyte binding<sup>1–5</sup> offering possibilities to use them as chemical sensors in biomedical research and as chemical logics<sup>6–8</sup> for molecular information processing. They usually consist of signaling (fluorophore) and guest-binding (receptor) moieties. The two components can either be separated by a spacer or can be integrated into one unit. The fluorophore, as such, does not show any selectivity. It is the receptor that should show selectivity and hence is the most difficult component to design. Systems with a spacer between the fluorophore and the receptor are versatile as modular chemistry principles can be applied to synthesize them. Using this approach, a variety of acyclic/cyclic receptors with one or more N donors linked covalently to the fluorophore have been reported<sup>1–8</sup> with intramolecular photoinduced electron transfer (PET) as the most commonly exploited mechanism.<sup>9</sup> In the absence of a guest, PET from the nitrogen lone-pair to the excited fluorophore takes place causing a nonradiative decay of the excited fluorophore and fluorescence quenching. Upon metal (guest) binding, the lone-pair is engaged, turning off the PET process and causing recovery of the fluorescence. Studies of photophysical behavior of such supramolecular systems are actively pursued to design efficient photodriven molecular/ionic sensors and switches besides understanding the mechanism of PET in greater detail. Design of efficient sensors/device systems in the format, “fluorophore–spacer–receptor” demands special molecular architecture that should fulfill certain important criteria which are as follows: (i) PET should be fast in the metal-free molecule,

(ii) PET should be effectively stopped once the guest is bonded to the receptor, (iii) the singlet  $\rightarrow$  triplet intersystem crossing efficiency should be poor, and (iv) the compound should be stable photochemically.

Transition metals are ubiquitous in biology and their detection in real-space and in real-time is, therefore, important for biological, clinical, as well as environmental interests. Besides, the ready availability of different oxidation states for these metals can be made use of in designing intelligent systems. However, these metals, especially the paramagnetic ones, are known quenchers. Blocking of their inherent quenching nature<sup>10</sup> requires that metal–receptor (M–R) interaction should be greater than the metal–fluorophore (M–F) communication. Several design principles are now available<sup>11</sup> to achieve this goal. We had earlier shown<sup>12</sup> that cryptands as receptors can be used for efficient fluorescent signaling of paramagnetic transition metals by shielding the metal inside the cavity from interacting with the fluorophore. Herein, we describe several systems (Figure 1) where one or more electron-withdrawing groups have been covalently linked to the receptor. This new design was adopted to probe the PET process and we show that if the PET can be maximized by structural modification of the supramolecular system, the quenching influence of the transition metal ion can be overcome for moderate concentration of the metal ion. Thus, structurally simple fluorescent signaling systems for transition metal ions can be built without paying much attention to the magnitude of M–F interactions. To probe the effect of orientational variation of the fluorophore and the receptor on the emission, the X-ray and theoretical structural studies are undertaken.

\* Address correspondence to this author. E-mail: pkb@iitk.ac.in

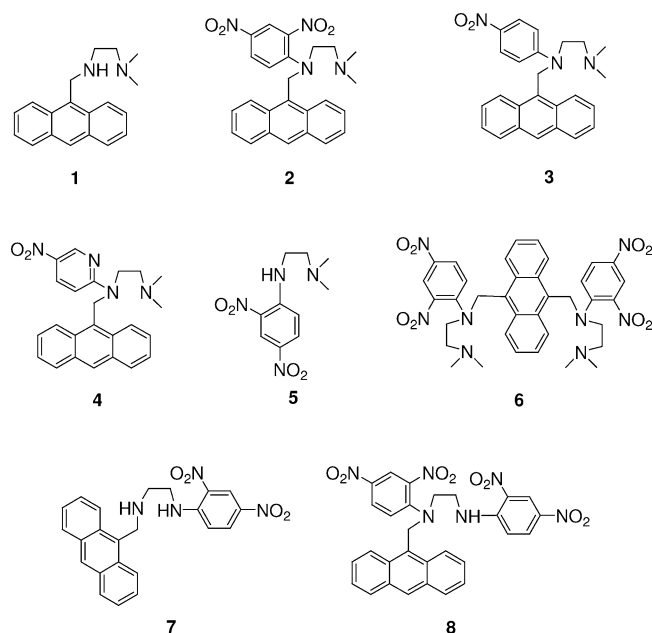


**Figure 1.** Chemical structures of the fluorophoric systems.

## 2. Experimental Section

**2.1. Methods.** Compounds **1–8** were synthesized as shown in Scheme 1, parts a–c. They were characterized by elemental analyses and  $^1\text{H}$  NMR,  $^{13}\text{C}$  NMR, and mass (positive ion) spectroscopy.  $^1\text{H}$  NMR and  $^{13}\text{C}$  NMR spectra were recorded on a JEOL JNM-LA400 FT (400 and 100 MHz, respectively) instrument in  $\text{CDCl}_3$ . FAB mass (positive ion) data were recorded on a JEOL SX 102/DA-6000 mass spectrometer using argon as the FAB gas at 6 kV and 10 mA with an accelerating voltage of 10 kV and the spectra were recorded at 298 K. Melting points were determined with an electrical melting point apparatus by PERFIT, India and were uncorrected. Elemental analyses were done in an Elementar Vario EL III Carlo Erba 1108 elemental analyzer. UV–visible spectra were recorded on a JASCO V-570 spectrophotometer at 293 K. Steady-state fluorescence spectra were obtained with a Perkin-Elmer LS 50B luminescence spectrometer at 293 K.

Fluorescence quantum yields of all the compounds except **5** were determined by comparing the corrected spectrum with that of anthracene ( $\phi = 0.297$ ) in ethanol<sup>13</sup> by taking the area under the total emission using the following equation<sup>14</sup>

$$\phi_S = \phi_R (F_S A_R / F_R A_S) (\eta_S / \eta_R)^2 \quad (1)$$

where  $\phi_S$  and  $\phi_R$  are the radiative quantum yields of the sample and the reference,  $F_S$  and  $F_R$  are the area under the fluorescence spectra of the sample and the reference,  $A_S$  and  $A_R$  are the absorbances of the sample and the reference (at the excited wavelength), and  $\eta_S$  and  $\eta_R$  are the refractive indices of the solvent used for the sample and the reference. The fluorescence quantum yield of **5** was determined through the above equation by comparing the corrected spectrum with that of quinine sulfate in 1 N  $\text{H}_2\text{SO}_4$ . The fluorescence measurements were carried out by using  $\sim 10^{-6}$  M solutions of the compounds unless otherwise specified.

The complex stability constant  $K_s$  were determined from the change in absorbance or fluorescence intensity resulting from the titration of dilute solutions ( $\sim 10^{-5}$ – $10^{-6}$  M) of the fluorophoric systems against metal ion solution. The linear fit of the fluorescence intensity data at a particular wavelength for

1:1 complexation was obtained by applying the following equation<sup>15</sup>

$$I_F^0 / (I_F - I_F^0) = [a/(b - a)] [(1/K_s[M]) + 1] \quad (2)$$

where  $I_F^0$  and  $I_F$  are the fluorescence intensity of the metal free ligand and the ML complex, respectively;  $[M]$  is the concentration of the metal ions added for complexation. The  $K_s$  is obtained as intercept/slope ratio from the plot of  $I_F^0 / (I_F - I_F^0)$  against  $[M]^{-1}$ . The change in absorption spectral data at a particular wavelength fitted into the following equation results in determination of  $K_s$ .

$$(A_0 - A) / (A - A_{\text{lim}}) = K_s [M] \quad (3)$$

$A_0$  and  $A$  are the absorbance of the metal-free ligand and the complexes, respectively. When  $(A_0 - A) / (A - A_{\text{lim}})$  is plotted against the metal ion concentration  $[M]$ ,  $K_s$  is directly obtained from the slope. The details of the theoretical analysis of the stoichiometries and corresponding binding constant determination are available<sup>15,16</sup> in the literature. Here the reported values are consistent with good correlation coefficients ( $\geq 0.99$ ).

**2.2. Materials.** Anthracene, 9-anthraldehyde, 1-chloro-2,4-dinitrobenzene, 4-fluoro-1-nitrobenzene, 2-chloro-5-nitropyridine, *N,N*-dimethylethylenediamine, and the metal salts were obtained from Aldrich and used as received. Ethylenediamine, triethylamine,  $\text{K}_2\text{CO}_3$ ,  $\text{NaBH}_4$ , paraformaldehyde, and *N*-methyl-2-pyrrolidone (NMP) were received from S. D. Fine, India. For chromatographic separation, 100–200 mesh silica gel (Acme Synthetic Chemicals) was used. All the solvents (S. D. Fine, India) and the amines were purified thoroughly prior to use for fluorescence measurements by following the literature<sup>17</sup> procedures. The purified solvents were found to be free from impurities and moisture and were transparent in the region of interest. All the reactions were carried out under  $\text{N}_2$  atmosphere unless otherwise mentioned. The metal salts  $\text{Zn}(\text{ClO}_4)_2(\text{H}_2\text{O})_6$ ,  $\text{Cu}(\text{ClO}_4)_2(\text{H}_2\text{O})_6$ ,  $\text{Ni}(\text{ClO}_4)_2(\text{H}_2\text{O})_6$ ,  $\text{Co}(\text{ClO}_4)_2(\text{H}_2\text{O})_6$ ,  $\text{Fe}(\text{ClO}_4)_2(\text{MeCN})_4$ ,  $\text{Mn}(\text{ClO}_4)_2(\text{H}_2\text{O})_6$ ,  $\text{Cd}(\text{ClO}_4)_2 \cdot \text{H}_2\text{O}$ , and  $\text{HClO}_4$  were used as ionic input for the photophysical studies.

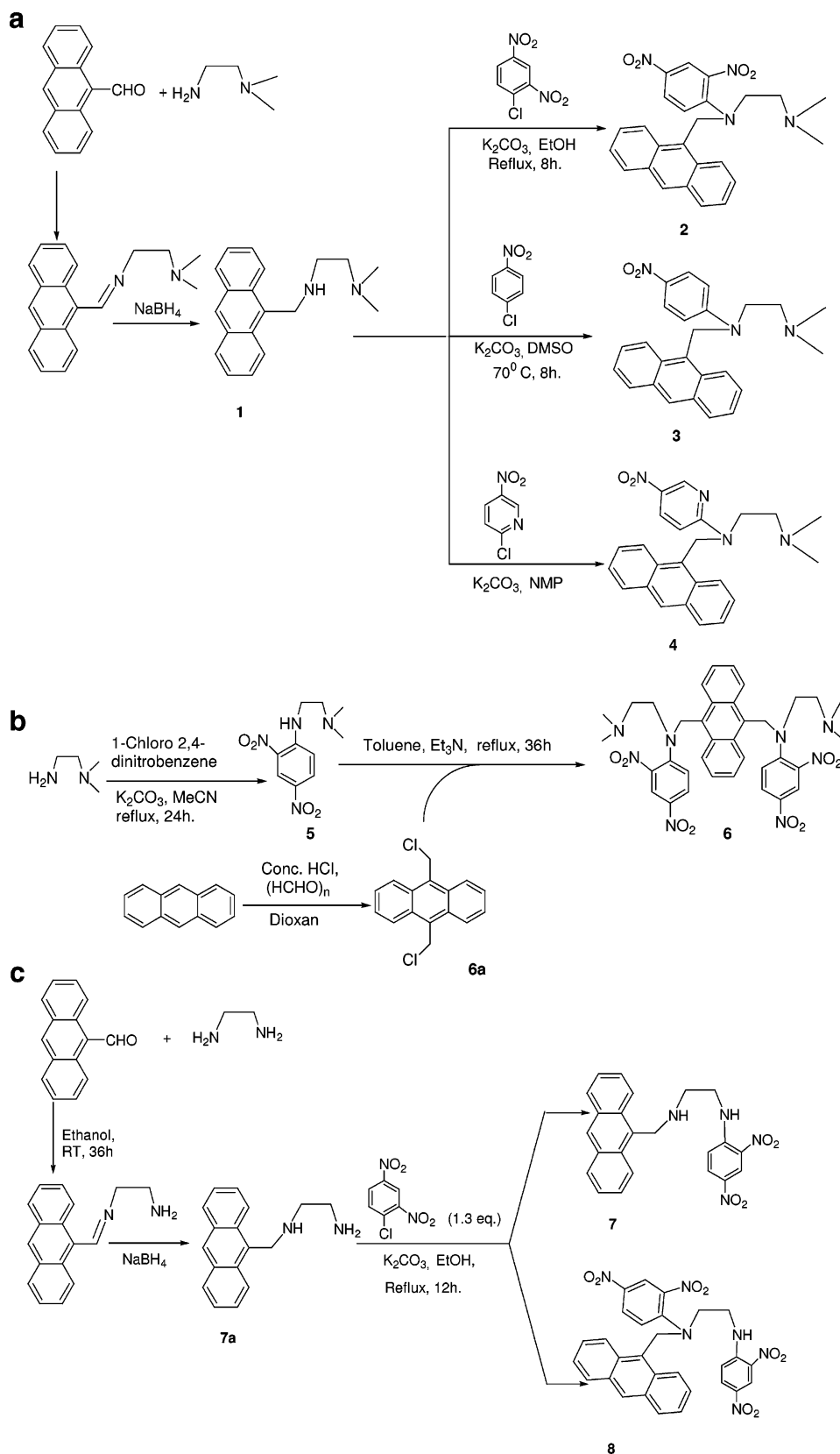
**2.3. Synthesis.** The synthetic routes adopted for the fluorescent signaling systems are given in Scheme 1.

*N,N*-Dimethyl-*N'*-(9-methylantraceny)ethylenediamine, **1**: To a solution of anthracene-9-carboxaldehyde (1.24 g; 6 mmol) in ethanol (70 mL) was added *N,N*-dimethylethylenediamine (0.7 mL; 6.6 mmol) and the solution was allowed to react for 36 h at room temperature with constant stirring. Solid  $\text{NaBH}_4$  (excess) was added and the mixture was heated to reflux for 4 h to reduce the Schiff base formed. After removal of the solvent under reduced pressure, the pale yellow solid remained and the solution was stirred with water (100 mL) for 30 min and extracted with DCM. The organic layer, after drying over anhydrous  $\text{Na}_2\text{SO}_4$ , was filtered and evaporated to dryness whereupon **1** was obtained as a brown semisolid.

Yield 92%;  $^1\text{H}$  NMR (400 MHz,  $\text{CDCl}_3$ , 25 °C, TMS,  $\delta$ ) 2.17 (s, 6H,  $2 \times \text{CH}_3$ ), 2.47 (t,  $J = 6.22$  Hz, 2H,  $\text{CH}_2$ ), 2.93 (t,  $J = 6.22$  Hz, 2H,  $\text{CH}_2$ ), 4.73 (s, 2H, An- $\text{CH}_2$ ), 5.23 (s, 1H, NH), 7.44 (t,  $J = 6.31$  Hz, 2H, An- $\text{H}_{2,7}$ ), 7.52 (t,  $J = 6.83$  Hz, 2H, An- $\text{H}_{3,6}$ ), 7.88 (d,  $J = 8.39$  Hz, 2H, An- $\text{H}_{4,5}$ ), 8.3 (m, 3H, An- $\text{H}_{1,8,10}$ );  $^{13}\text{C}$  NMR (100 MHz,  $\text{CDCl}_3$ , 25 °C, TMS,  $\delta$ ) 131.6, 131.4, 130, 129, 127, 125.9, 124.8, 124.1, 58.7, 47.5, 45.5, 45.2; FAB-MS ( $m/z$ ) 279 (34%)  $[\text{M} + 1]^+$ . Anal. Calcd for  $\text{C}_{19}\text{H}_{22}\text{N}_2$ : C, 81.97; H, 7.97; N, 10.06. Found: C, 81.73; H, 8.07; N 9.91.

*N,N*-Dimethyl[*N'*-(9-methylantraceny)-*N'*-(2,4-dinitrophenyl)]ethylenediamine, **2**: To a clear solution of **1** (1.36 g; 5

## SCHEME 1: Synthetic Route to the Investigated Compounds



mmol) in ethanol (30 mL) was added  $K_2CO_3$  (0.83 g; 6 mmol) and the solution was refluxed for 15 min with constant stirring. A solution of 1-chloro-2,4-dinitrobenzene (1.0 g; 5 mmol) in ethanol (20 mL) was added in drops to the stirring solution and reflux continued for 8 h. The reaction mixture was then brought to room temperature and the solvent distilled off under reduced

pressure to obtain a yellow solid. This solid was stirred for 30 min in water (100 mL) and extracted with  $CHCl_3$ . The organic layer, after drying over anhydrous  $Na_2SO_4$ , was evaporated to dryness to obtain the desired product, **2**. This was purified through column chromatography (100–200 mesh silica gel) with DCM and ethyl acetate (1:1 v/v) as the eluent and isolated as

a pale yellow solid, which crystallizes from MeCN or DCM as pale yellow blocks.

Yield 70(%); mp 165 °C;  $^1\text{H}$  NMR (400 MHz,  $\text{CDCl}_3$ , 25 °C, TMS,  $\delta$ ) 1.95 (s, 6H,  $2 \times \text{CH}_3$ ), 2.25 (t,  $J = 6.95$  Hz, 2H,  $\text{CH}_2$ ), 3.12 (t,  $J = 6.95$  Hz, 2H,  $\text{CH}_2$ ), 5.09 (s, 2H, An- $\text{CH}_2$ ), 7.25 (d,  $J = 9.51$  Hz, 1H, Ph- $\text{H}_6$ ), 7.46 (m, 4H, An- $\text{H}_{2,3,6,7}$ ), 7.89 (d,  $J = 9.03$  Hz, 2H, An- $\text{H}_{4,5}$ ), 7.99 (d,  $J = 7.55$  Hz, 2H, An- $\text{H}_{1,8}$ ), 8.24 (dd,  $J = 2.68$  Hz,  $J = 9.27$  Hz, 1H, Ph- $\text{H}_5$ ), 8.45 (s, 1H, An- $\text{H}_{10}$ ), 8.8 (s, 1H, Ph- $\text{H}_3$ );  $^{13}\text{C}$  NMR (100 MHz,  $\text{CDCl}_3$ , 25 °C, TMS,  $\delta$ ) 149.38, 137.66, 131.2, 129.3, 127.15, 127.76, 125.43, 124.38, 123.14, 119.60, 57.12, 49.77, 47.09, 45.08; FAB-MS ( $m/z$ ) 444.489 (65%) [ $\text{M}$ ] $^+$ . Anal. Calcd for  $\text{C}_{25}\text{H}_{24}\text{N}_4\text{O}_4$ : C, 67.56; H, 5.44; N, 12.61. Found: C, 67.38; H, 5.59; N, 12.53.

*N,N*-Dimethyl[*N'*-(9-methylanthracenyl)-*N'*-(4-nitrophenyl)]ethylenediamine, **3**: To a completely dissolved solution of **1** (0.54 g; 2 mmol) in DMSO was added  $\text{K}_2\text{CO}_3$  (0.33 g; 2.4 mmol) with stirring for 15 min at room temperature. Neat 4-fluoro-1-nitrobenzene (0.2 mL; 2 mmol) was added and the solution was allowed to react for 48 h at 70 °C with constant stirring. A yellow precipitate was deposited at the bottom, collected by filtration, and washed with plenty of water. The compound was dissolved in  $\text{CHCl}_3$  and the  $\text{CHCl}_3$  layer was washed six times with water. The organic layer after, drying over anhydrous  $\text{Na}_2\text{SO}_4$ , was evaporated to dryness to obtain a brown semisolid, which was further purified by passing through a column (100–200 mesh silica gel) with an ethyl acetate and dichloromethane mixture (30:70 v/v) as the eluent. The desired product was obtained as yellow crystals from acetonitrile.

Yield 79(%); mp 181 °C;  $^1\text{H}$  NMR (400 MHz,  $\text{CDCl}_3$ , 25 °C, TMS,  $\delta$ ) 1.65 (s, 6H,  $2 \times \text{CH}_3$ ), 2.01 (t,  $J = 7.93$  Hz, 2H,  $\text{CH}_2$ ), 3.11 (t,  $J = 7.91$  Hz, 2H,  $\text{CH}_2$ ), 5.32 (s, 2H, An- $\text{CH}_2$ ), 6.92 (d,  $J = 9.51$  Hz, 2H, Ph- $\text{H}_{2,6}$ ), 7.52 (m, 4H, An- $\text{H}_{2,3,6,7}$ ), 8.03 (m, 4H, An- $\text{H}_{1,4,5,8}$ ), 8.21 (d,  $J = 7.31$  Hz, 2H, Ph- $\text{H}_{3,5}$ ), 8.5 (s, 1H, An- $\text{H}_{10}$ );  $^{13}\text{C}$  NMR (100 MHz,  $\text{CDCl}_3$ , 25 °C, TMS,  $\delta$ ) 153.22, 137.52, 131.37, 131.24, 129.41, 128.99, 127.05, 126.45, 125.72, 125.28, 123.55, 110.91, 55.74, 45.51, 44.97, 44.44; FAB-MS ( $m/z$ ) 400 (65%) [ $\text{M}$ ] $^+$ . Anal. Calcd for  $\text{C}_{25}\text{H}_{25}\text{N}_3\text{O}_2$ : C, 75.16; H, 6.31; N, 10.52. Found: C, 75.01; H, 6.39; N, 10.48.

*N,N*-Dimethyl[*N'*-(9-methylanthracenyl)-*N'*-(5-nitropyridyl)]ethylenediamine, **4**: To a solution of **1** (0.54 g; 2 mmol) in dry *N*-methyl-2-pyrrolidone (NMP, 20 mL) was added triethylamine (0.42 mL; 3 mmol) over a period of 15 min with constant stirring. A solution of 2-chloro-5-nitropyridine (0.32 g; 2 mmol) in NMP (10 mL) was added dropwise for 1 h and then allowed to react for 36 h at 70 °C with constant stirring. The reaction mixture, after bringing it back to room temperature, was poured into cold water. A pale yellow solid crushed out, which was collected by filtration. The solid was washed with plenty of water and dried, then further purified by passing through a column (100–200 mesh silica gel) with an ethyl acetate and dichloromethane mixture (7:93 v/v) as the eluent. The desired product thus obtained easily crystallizes from ethyl acetate solution as yellow needles suitable for single-crystal X-ray diffraction.

Yield 75(%); mp 189 °C;  $^1\text{H}$  NMR (400 MHz,  $\text{CDCl}_3$ , 25 °C, TMS,  $\delta$ ) 1.79 (s, 6H,  $2 \times \text{CH}_3$ ), 2.01 (t,  $J = 7.79$  Hz, 2H,  $\text{CH}_2$ ), 3.33 (t,  $J = 7.79$  Hz, 2H,  $\text{CH}_2$ ), 5.92 (s, 2H, An- $\text{CH}_2$ ), 6.71 (d,  $J = 9.51$  Hz, 1H, Ph- $\text{H}_3$ ), 7.50 (m, 4H, An- $\text{H}_{2,3,6,7}$ ), 8.03 (d,  $J = 9.47$  Hz, 2H, An- $\text{H}_{4,5}$ ), 8.20 (d,  $J = 8.51$  Hz, 2H, An- $\text{H}_{1,8}$ ), 8.28 (dd,  $J = 2.68$  Hz,  $J = 9.39$  Hz, 1H, Ph- $\text{H}_5$ ), 8.50 (s, 1H, An- $\text{H}_{10}$ ), 9.23 (s, 1H, Ph- $\text{H}_6$ );  $^{13}\text{C}$  NMR (100 MHz,  $\text{CDCl}_3$ , 25 °C, TMS,  $\delta$ ) 160.0, 146.6, 135.4, 133.3, 131.4 (d),

129.4, 128.8, 127.0, 126.7, 125.3, 123.7, 104.9, 55.4, 44.6, 43.5, 43.2; FAB-MS ( $m/z$ ) 400 (70%) [ $\text{M}$ ] $^+$ . Anal. Calcd for  $\text{C}_{24}\text{H}_{24}\text{N}_4\text{O}_2$ : C, 71.98; H, 6.04; N, 13.99. Found: C, 71.51; H, 6.29; N, 13.91.

*N,N*-Dimethyl-*N'*-(2,4-dinitrophenyl)ethylenediamine, **5**: To a stirring solution of *N,N*-dimethylethylenediamine (0.55 mL; 5 mmol) in ethanol (40 mL) was added anhydrous  $\text{K}_2\text{CO}_3$  (0.83 g; 6 mmol) followed by dropwise addition of an ethanolic solution of 1-chloro-2,4-dinitrobenzene (1.0 g; 5 mmol). The mixture was heated to reflux for 16 h whereupon orange solids were precipitated out. The reaction mixture, after cooling to room temperature, was filtered off and the residue stirred with water for 1 h to remove  $\text{K}_2\text{CO}_3$ . The orange solid thus obtained was recrystallized from ethanol to obtain the desired product as orange rectangular parallelepiped crystals suitable for single-crystal X-ray diffraction.

Yield 91(%); mp 66 °C;  $^1\text{H}$  NMR (400 MHz,  $\text{CDCl}_3$ , 25 °C, TMS,  $\delta$ ) 2.29 (s, 6H,  $2 \times \text{CH}_3$ ), 2.64 (t,  $J = 6.12$  Hz, 2H,  $\text{CH}_2$ ), 3.39 (q,  $J = 4.88$  Hz, 2H,  $\text{CH}_2$ ), 6.85 (d,  $J = 9.51$  Hz, 1H, Ph- $\text{H}_6$ ), 8.20 (dd,  $J = 2.28$  Hz,  $J = 9.51$  Hz, 1H, Ph- $\text{H}_5$ ), 8.94 (br, s, 1H, NH), 9.05 (s, 1H, Ph- $\text{H}_3$ );  $^{13}\text{C}$  NMR (100 MHz,  $\text{CDCl}_3$ , 25 °C, TMS,  $\delta$ ) 40.83, 44.96, 56.52, 114.14, 124.17, 130.13, 135.64, 148.06. FAB-MS ( $m/z$ ) 254 (100%) [ $\text{M}$ ] $^+$ . Anal. Calcd for  $\text{C}_{10}\text{H}_{14}\text{N}_4\text{O}_4$ : C, 47.24; H, 5.55; N, 22.04. Found: C, 47.15; H, 5.59; N, 21.91.

9,10-Bis(chloromethyl)anthracene, **6a**: This compound was prepared as per the procedure reported<sup>18</sup> earlier by Miller et al. The yellow solid obtained was recrystallized from toluene.

Yield 92 (%); mp 254–256 °C;  $^1\text{H}$  NMR (400 MHz,  $d_6$ -acetone, 25 °C, TMS,  $\delta$ ) 5.70 (s, 4H,  $2 \times \text{CH}_2$ ), 7.60 (m, 4H, An- $\text{H}_{2,3,6,7}$ ), 8.40 (m, 4H, An- $\text{H}_{1,4,5,8}$ ). Anal. Calcd for  $\text{C}_{16}\text{H}_{12}\text{Cl}_2$ : C, 69.84; H, 4.40. Found: C, 69.69; H, 4.29.

9,10-Bis(aminoethyl)[*N,N*-dimethyl-*N'*-(2,4-dinitrophenyl)aminoethyl]anthracene, **6**: To a stirring solution of **5** (1.0 g; 4 mmol) in toluene (40 mL) was added triethylamine (0.56 mL; 4 mmol) and the solution was warmed at 50 °C for 30 min. A solution of 9,10-bis(chloromethyl)anthracene (0.55 g; 2 mmol) in toluene (30 mL) was added dropwise and then heated to reflux for 48 h. The solvent was removed under reduced pressure and the solid remaining was stirred with water (50 mL) and then extracted with ethyl acetate. The organic layer, after drying over  $\text{Na}_2\text{SO}_4$ , was evaporated to dryness to obtain the desired product as a brown solid. Yield 86(%); mp 161 °C;  $^1\text{H}$  NMR (400 MHz,  $\text{DMSO}-d_6$ , 25 °C, TMS,  $\delta$ ) 3.05 (s, 12H,  $4 \times \text{CH}_3$ ), 4.14 (br, s, 4H,  $2 \times \text{CH}_2$ ), 4.21 (br, s, 4H,  $2 \times \text{CH}_2$ ), 5.93 (s, 4H,  $2 \times \text{An-CH}_2$ ), 7.45 (d, 2H,  $2 \times \text{Ph-H}_6$ ), 7.72 (m, 4H, An- $\text{H}_{2,3,6,7}$ ), 8.24 (d, 2H,  $2 \times \text{Ph-H}_5$ ), 8.85 (d, 2H, An- $\text{H}_{4,5}$ ), 8.90 (d, 2H, An- $\text{H}_{1,8}$ ), 9.04 (d, 2H,  $2 \times \text{Ph-H}_3$ );  $^{13}\text{C}$  NMR (100 MHz,  $\text{DMSO}-d_6$ , 25 °C, TMS,  $\delta$ ) 147.66, 135.43, 132.71, 130.57, 129.92, 127.09, 125.80, 124.11, 123.46, 115.89, 62.76, 58.63, 49.80, 37.17; FAB-MS ( $m/z$ ) 747 (77%) [ $\text{M} + 1.2\text{H}_2\text{O}$ ] $^+$ . Anal. Calcd for  $\text{C}_{36}\text{H}_{38}\text{N}_8\text{O}_8$ : C, 60.84; H, 5.39; N, 15.77. Found: C, 60.75; H, 5.67; N, 15.69.

*N*-(9-Methylanthracenyl)ethylenediamine, **7a**: To a stirring solution of anthracene 9-carbaldehyde (1.0 g; 5 mmol) in ethanol (70 mL) was added ethylenediamine (1.7 mL; 25 mmol) and the solution was allowed to react for 36 h at room temperature with constant stirring. The Schiff base thus formed was reduced by adding solid  $\text{NaBH}_4$  (excess) to it. The mixture was further heated at 50 °C for 2 h to ensure a complete reduction of the imine formed. The solvent was distilled off under reduced pressure, the solid was stirred with 50 mL of water, and the product was extracted with  $\text{CHCl}_3$  ( $3 \times 30$  mL). The organic layer, after drying over anhydrous  $\text{Na}_2\text{SO}_4$ , was evaporated to

dryness to obtain a brown semisolid, which was purified by passing through a column (silica gel 100–200 mesh) with a chloroform and methanol mixture (98:2 v/v) as the eluent. The desired product was obtained as a brown semisolid.

Yield 82(%);  $^1\text{H}$  NMR (400 MHz,  $\text{CDCl}_3$ , 25 °C, TMS  $\delta$ ) 2.74 (t,  $J = 5.36$  Hz, 2H,  $\text{CH}_2$ ), 2.80 (t,  $J = 5.36$  Hz, 2H,  $\text{CH}_2$ ), 3.62 (br, s, 3H), 4.53 (s, 2H, An- $\text{CH}_2$ ), 7.32 (t,  $J = 7.79$  Hz, 2H, An- $\text{H}_{2,7}$ ), 7.43 (t,  $J = 8.51$  Hz, 2H, An- $\text{H}_{3,6}$ ) 7.81 (d,  $J = 8.27$  Hz, 2H, An- $\text{H}_{4,5}$ ), 8.18 (d,  $J = 7.56$  Hz, 2H, An- $\text{H}_{1,8}$ ), 8.21 (s, 1H, An- $\text{H}_{10}$ );  $^{13}\text{C}$  NMR (100 MHz,  $\text{CDCl}_3$ , 25 °C, TMS,  $\delta$ ) 131.27, 131.11, 130.05, 128.91, 127.06, 126.01, 124.78, 123.94, 50.88, 45.14, 40.73; FAB-MS ( $m/z$ ) 251 (64%) [ $\text{M}$ ] $^+$ . Anal. Calcd for  $\text{C}_{17}\text{H}_{18}\text{N}_2$ : C, 81.56; H, 7.25; N, 11.19. Found: C, 81.51; H, 7.32; N, 11.11.

Compounds **7** and **8** were prepared by controlled substitution of 1-chloro-2,4-dinitrobenzene with **7a**. The amine **7a** (1.25 g, 5 mmol) was dissolved in ethanol (50 mL),  $\text{K}_2\text{CO}_3$  (0.9 g; 6.5 mmol) was added to the solution, and the mixture was stirred for 15 min. An ethanolic solution of 1-chloro-2,4-dinitrobenzene (1.2 g; 6.5 mmol) was added dropwise to the stirring solution which was heated to reflux for 12 h. The solvent was removed from the reaction mixture under reduced pressure. After addition of water (100 mL), it was extracted with  $\text{CHCl}_3$  (3  $\times$  30 mL). The organic layer, after drying over anhydrous  $\text{Na}_2\text{SO}_4$ , was evaporated to dryness to obtain a mixture of the desired products **7** and **8** as a yellow solid. These compounds were separated and purified by silica gel column chromatography (silica gel, 100–200 mesh) with a chloroform and methanol mixture as eluent.

*N*-[(2,4-Dinitrophenyl)(9-methylanthracenyl)]-*N'*-(2,4-dinitrophenyl)ethylenediamine, **8**: This compound was eluted out first with chloroform:methanol in 99:1 (v/v) as the eluent. This product was isolated as a yellow solid, which crystallizes as yellow crystals suitable for single-crystal X-ray diffraction upon slow evaporation of a DMSO and ethyl acetate mixed solution.

Yield 35(%); mp: 198 °C;  $^1\text{H}$  NMR (400 MHz,  $\text{DMSO}-d_6$ , 25 °C, TMS,  $\delta$ ) 3.1 (q,  $J = 5.36$  Hz, 2H,  $\text{CH}_2$ ), 3.2 (t,  $J = 5.42$  Hz, 2H,  $\text{CH}_2$ ), 5.44 (s, 2H, An- $\text{CH}_2$ ), 7.3 (d,  $J = 9.26$  Hz, 2H, Ph- $\text{H}_6$ ), 7.43 (d,  $J = 8.27$  Hz, 2H, An- $\text{H}_{2,7}$ ), 7.88 (m, 4H, An- $\text{H}_{3,6,4,5}$ ), 8.12 (s, 1H, An- $\text{H}_{10}$ ), 8.3 (d,  $J = 9.75$  Hz, 2H, Ph- $\text{H}_5$ ), 8.64 (d,  $J = 8.51$  Hz, 2H, An- $\text{H}_{1,8}$ ), 8.76 (s, 2H, Ph- $\text{H}_3$ );  $^{13}\text{C}$  NMR (100 MHz,  $\text{DMSO}-d_6$ , 25 °C, TMS,  $\delta$ ) 146.6, 145.0, 138.3, 137.2, 133.3, 131.2, 131.0, 130.7, 129.4, 129.1, 128.8, 127.5, 126.3, 125.1, 124.7, 123.9, 119.5, 114.2, 56.4, 55.9, 47.0; FAB-MS ( $m/z$ ) 583 (100%) [ $\text{M}$ ] $^+$ . Anal. Calcd for  $\text{C}_{29}\text{H}_{22}\text{N}_6\text{O}_8$ : C, 59.79; H, 3.81; N, 14.43. Found: C, 59.68; H, 3.72; N, 14.28.

*N*-(9-Methylanthracenyl)-*N'*-(2,4-dinitrophenyl)ethylenediamine, **7**: This compound was eluted out next with chloroform:methanol in 97:3 (v/v) as the eluent. This product was isolated as a brown solid, which crystallizes as prismatic brown crystals upon slow diffusion of chloroform into the ethanol solution.

Yield 60(%); mp 172 °C;  $^1\text{H}$  NMR (400 MHz,  $\text{DMSO}-d_6$ , 25 °C, TMS,  $\delta$ ) 3.03 (t,  $J = 5.84$  Hz, 2H,  $\text{CH}_2$ ), 3.51 (t,  $J = 5.12$  Hz, 2H,  $\text{CH}_2$ ), 4.63 (s, 2H, An- $\text{CH}_2$ ), 7.09 (d,  $J = 9.51$  Hz, 1H, Ph- $\text{H}_6$ ), 7.45 (m, 4H, An- $\text{H}_{2,3,6,7}$ ), 8.00 (d,  $J = 9.03$  Hz, 2H, An- $\text{H}_{4,5}$ ), 8.11 (dd,  $J = 2.68$  Hz,  $J = 9.75$  Hz, 1H, Ph- $\text{H}_5$ ), 8.37 (d,  $J = 9.43$  Hz, 2H, An- $\text{H}_{1,8}$ ), 8.46 (s, 1H, An- $\text{H}_{10}$ ), 8.76 (s, 1H, Ph- $\text{H}_3$ ), 8.94 (br, s, 1H, NH);  $^{13}\text{C}$  NMR (100 MHz,  $\text{DMSO}-d_6$ , 25 °C, TMS,  $\delta$ ) 131.87, 131.01, 129.96, 129.78, 129.38, 128.72, 126.68, 125.78, 125.05, 124.81, 123.56, 115.58, 47.25, 44.51, 42.45; FAB-MS ( $m/z$ ) 417 (53%) [ $\text{M}$ ] $^+$ . Anal. Calcd for  $\text{C}_{23}\text{H}_{20}\text{N}_4\text{O}_4$ : C, 66.34; H, 4.84; N, 13.45. Found: C, 66.29; H, 4.71; N, 13.26.

**2.4. X-ray Crystallography.** Single-crystal X-ray diffraction data for **2**, **3**, **4**, **5**, **7**, and **8** were collected on an Enraf Nonius CAD4 Mach2 diffractometer with graphite-monochromated  $\text{Mo K}\alpha$  radiation ( $\lambda = 0.71073$  Å) at 273 K. The cell parameters in each case were determined by least-squares refinement of the diffractometer setting angles from 25 centered reflections that were in the range  $20^\circ \leq 2\theta \leq 25^\circ$ . Three standard reflections were measured every hour to monitor instrument and crystal stability during intensity data collection. The linear absorption coefficients, scattering factors for the atoms, and the anomalous dispersion corrections were taken from International Tables for X-ray Crystallography.<sup>19</sup> The structures were solved by the direct method using SIR97<sup>20</sup> and were refined on  $F^2$  by full-matrix least-squares technique using the SHELXL-97 program package.<sup>21</sup> In each case, some of the H atoms could be located in the difference maps while the rest were calculated assuming ideal geometries of the atoms concerned. All non-hydrogen atoms were refined anisotropically while the hydrogens were treated as riding atoms using SHELXL default parameters.

### 3. Results and Discussion

**3.1. Crystallographic Structural Studies.** Perspective views of the compounds showing the atom numbering schemes are given in Figure 2 for **2**, **3**, **4**, **5**, **7**, and **8**. Selected bond lengths, bond angles, and dihedral angles for the compounds are collected in Table 1. Attachment of electron-withdrawing groups to the receptor has made a significant contribution to the stereoelectronic situation in the molecules. The N2–C5 bond is much shorter (range, 1.346–1.371 Å) than the normal C–N bond (e.g., average N1–C3 bond length, 1.450 Å) in all the structures. This is due to delocalization of electron density from N2 to the attached electron-withdrawing aromatic  $\pi$  system inducing a partial double bond character of the N2–C5 bond. The solid-state structures reveal that restricted rotation around the N2–C5 bond results in a different spatial relationship among the fluorophore, the receptor, and the electron-withdrawing moieties in these molecules. The torsion angles  $\theta_1$ ,  $\theta_2$ , and  $\theta_3$  (Table 1) vary widely for the structures. However, the angle  $\theta_4$  deviates only a few degrees from the ideal planar orientation in **2**, **4**, and **8** although in **3** and **5** the angle is significantly twisted with respect to N2. For **7**, N2–C3 (1.337 Å) exhibits a partial double bond character because of the attached 2,4-dinitrobenzene group. The N2–C2–C1–N1 unit is very much deviated (torsion angle,  $51.0^\circ$ ) from planarity due to the presence of 2,4-dinitrobenzene and the anthracene moieties at the two ends of the receptor unit. The value of the angle  $\theta_3$  shows that the conformation of the anthracene ring with respect to N2 does not vary much in the structures. This shows that the pyramidal nature of the N2 atom does not significantly deviate from the normal geometry at least in the solid state. These structures show that the electron-withdrawing aromatic ring contributes more to the conformational changes through the N2–C5 bond. However, the crystal structures are favored by the packing forces rather than by the intrinsic differences in free energies. It might be suspected that the systems may have different geometries in solution. However, a comparison with simple AM1 calculations shows that the energy minimized structures (molecules in the gaseous phase) and the solid-state structures (molecules in the crystalline state) are in good overall agreement although subtle differences exist. However, solid-state structures of **5** and **8** differ from the energy minimized structures. In the case of **5**, the crystal structure shows extensive intra- as well as intermolecular H-bonding which are absent in other molecules whereas in the case of **8**, the structure is further stabilized by the solvent molecule present in the lattice.

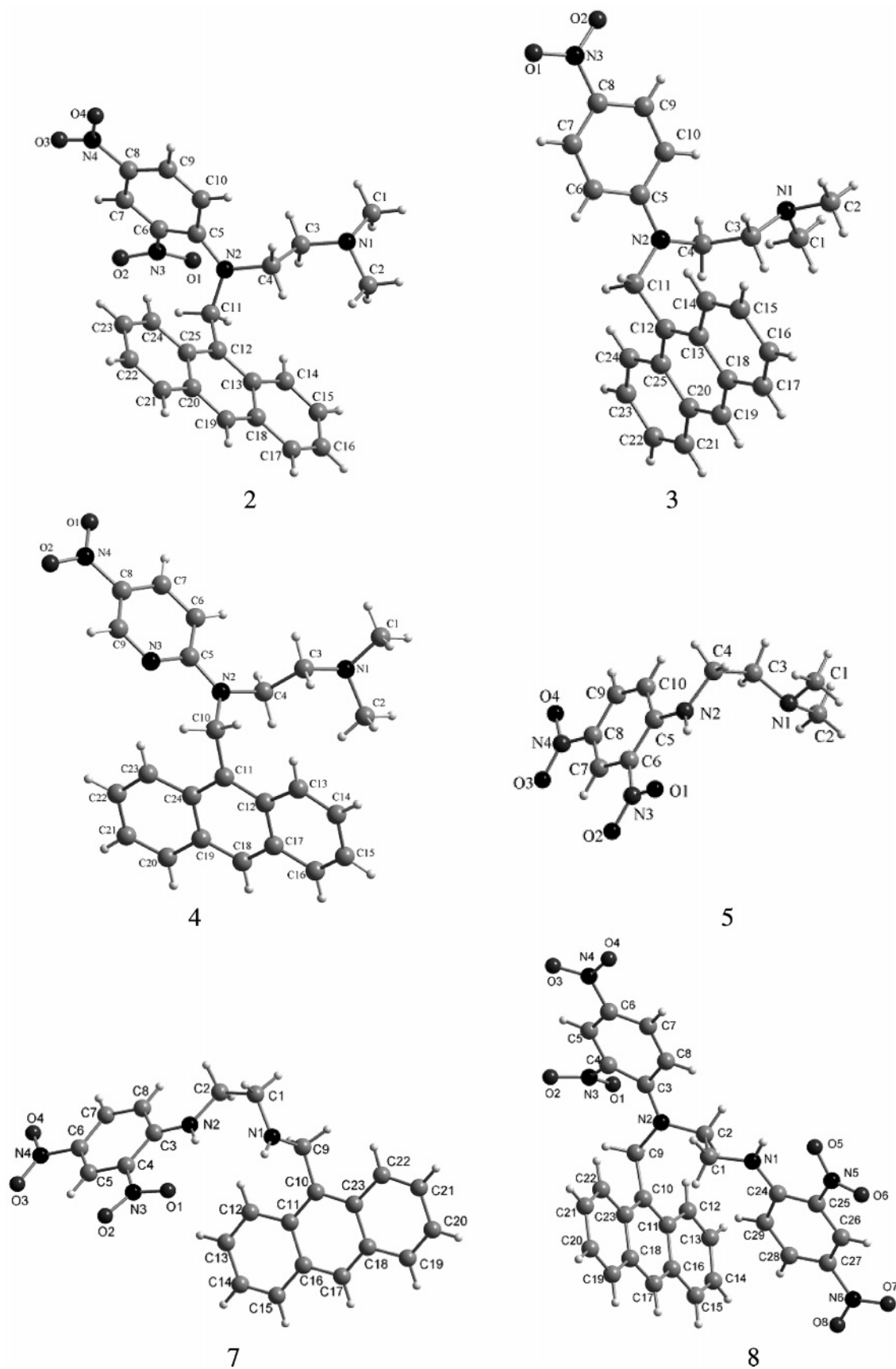


**Figure 2.** Perspective views of the X-ray structures of **2**, **3**, **4**, **5**, **7**, and **8** showing the atom numbering scheme.

**3.2. UV–Vis Spectroscopy.** Compound **1** in dry THF exhibits<sup>22</sup> the (0,0) band at 385 nm with vibrational structures at 366, 348, and 331 nm characteristic<sup>13</sup> of mono 9-alkyl substituted anthracene. This suggests the absence of any

interaction between the N lone-pair of the receptor and the anthracene group in the ground state. These transitions do not exhibit any significant solvatochromic behavior. The absorption spectrum of **2** in dry THF shows transitions at 393, 373, 355,

**TABLE 1: Selected Bond Distances (Å), Bond Angles (deg), and Torsional Angles (deg) of the Structures<sup>a</sup> 5, 2, 3, 4, and 8**

parameter	5	2	3	4 <sup>b</sup>	8 <sup>c</sup>
N2–C5 ( $b_1$ )	1.346(5)	1.352(3)	1.371(2)	1.357(4)	1.356(4)
N2–C4 ( $b_2$ )	1.452(5)	1.464(3)	1.463(2)	1.449(5)	1.469(4)
N2–C11 ( $b_3$ )		1.471(3)	1.478(2)	1.470(4)	1.480(4)
N2–C5–C6 ( $\alpha_1$ )	122.6 (4)	123.7(2)	121.9(1)	116.5(3)	124.8(3)
C4–N2–C5 ( $\alpha_2$ )	123.7(3)	121.5(2)	119.1(1)	122.2(3)	119.5(2)
C4–N2–C11 ( $\alpha_3$ )		116.7(2)	120.2(1)	117.0(3)	118.1(2)
C4–N2–C5–C10 ( $\theta_1$ )	–5.8(6)	–30.4(3)	–15.6(3)	0.0(5)	–17.7(4)
C11–N2–C5–C10 ( $\theta_2$ )		150.6(2)	178.4(2)	174.0(4)	162.1(3)
N2–C11–C12–C13 ( $\theta_3$ )		–106.0(3)	77.7(2)	107.5(4)	–104.7(3)
N1–C3–C4–N2 ( $\theta_4$ )	–74.4(4)	–178.5(2)	–143.5(2)	–179.9(3)	–170.2(2)
C4–N2–C11–C12 ( $\theta_5$ )		56.8(3)	26.0(2)	–50.1(4)	36.5(4)

<sup>a</sup> Crystallographic data and structural refinement of these structures are given in the Supporting Information. <sup>b</sup> For **4**, the parameters are  $b_3 = \text{N2–C10}$ ,  $\alpha_1 = \text{N2–C5–N3}$ ,  $\theta_2 = \text{C10–N2–C5–C6}$ ,  $\theta_3 = \text{N2–C10–C11–C12}$ . <sup>c</sup> For **8**, the parameters are  $b_1 = \text{N2–C3}$ ,  $b_2 = \text{N2–C2}$ ,  $b_3 = \text{N2–C9}$ ,  $\alpha_1 = \text{N2–C3–C4}$ ,  $\alpha_2 = \text{C3–N2–C2}$ ,  $\alpha_3 = \text{C2–N2–C9}$ ,  $\theta_1 = \text{C2–N2–C3–C8}$ ,  $\theta_2 = \text{C9–N2–C3–C8}$ ,  $\theta_3 = \text{N2–C9–C10–C11}$ ,  $\theta_4 = \text{N1–C1–C2–N2}$ ,  $\theta_5 = \text{C2–N2–C9–C10}$  as per the numbering scheme.

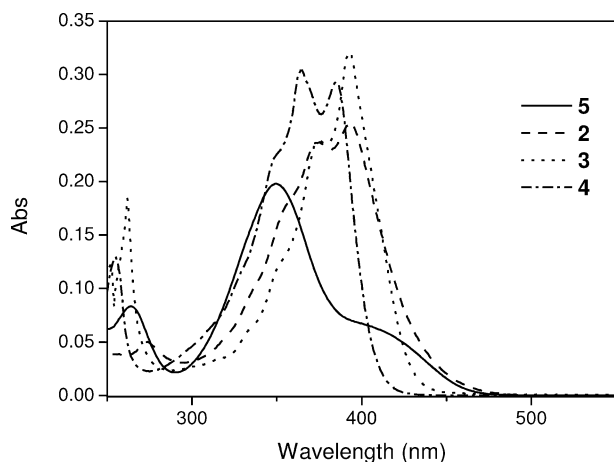


**Figure 3.** Absorption spectra of **2**, **3**, **4**, and **5** in THF at  $1 \times 10^{-5}$  M concentration.

and 274 nm. The peak at 274 nm is attributable<sup>23</sup> to the transition originating from interaction of the phenyl and the anthracene  $\pi$  systems in the ground state. The absorptions between 350 and 400 nm are due to a combination of two different types of transitions: (i) intramolecular charge transfer from the donor N-atom to the acceptor nitro groups separated through a  $\pi$ -spacer and (ii) structured anthracene-localized  $\pi \rightarrow \pi^*$  transitions. These transitions overlap each other in **2** as can be ascertained from the shape of the bands. The spectral features of compounds **3** and **4** are similar to those of **2** (Figure 3).

To understand the processes and the extent of contributions from the electron-withdrawing group, the D– $\pi$ –A ligand system **5** was synthesized. The absorption peak observed for this compound centered at 354 nm in dry THF is assignable<sup>24</sup> as the intramolecular charge transfer (ICT) transition from the donor N-atom to the nitro acceptor. A slightly red-shifted broad band at 414 nm is also observed, which may be due to another charge-transfer transition through space, occurring between the distal dimethyl substituted N-atom and the acceptor. The ICT transition at 354 nm is found to be solvatochromic<sup>25</sup> in nature: it absorbs at 330 nm in nonpolar hexane and at 363 nm in a relatively polar DMSO (Figure 4). Compound **6** exhibits prominent transitions at 393, 351, and 251 nm which are assignable as a combination of 9,10-dialkyl substituted anthracene and the ICT transition as in case of **2–4**.

The *N,N*-dimethylamino group here plays a vital role in the ICT-PET combined processes by effectively stabilizing the excited polar state. To investigate the role of this electron-donating dimethylamino group on the photophysical properties

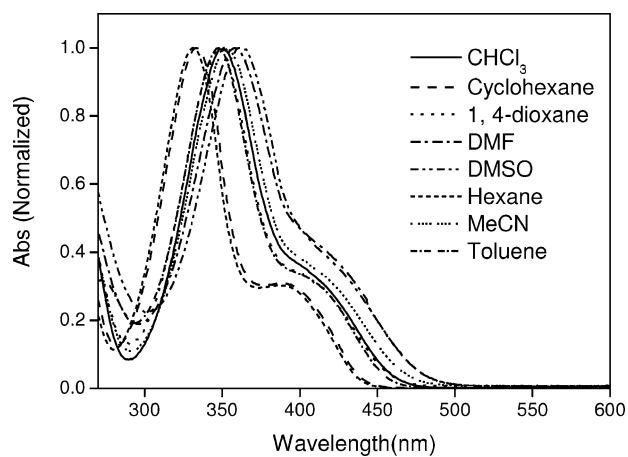


**Figure 4.** Absorption spectra (normalized) of **5** in different solvents.

of these systems and to resolve the role of each kind of process, compounds **7** and **8** were synthesized where the electron-donating methyl groups are replaced by the electron-withdrawing 2,4-dinitrobenzene group (Figure 1). In **7**, the charge transfer and electron transfer processes occur simultaneously within the same molecule but not from the same N atom. The transitions due to ICT and anthracene  $\pi \rightarrow \pi^*$  occur at 384, 365, 349, and 260 nm, which are blue-shifted in comparison to the transitions for compounds **2**, **3**, and **4**, where charge-transfer and electron-transfer processes occur from the same donor N atom. In **8**, an additional electron withdrawing 2,4-dinitrobenzene group is attached to the same donor N atom of **7** to which the fluorophoric unit is attached. The absorption peaks in **8** are observed at 393, 373, 356, and 256 nm which are red-shifted in comparison to those of **7**. It follows, therefore, that the absorption band shifts to lower energy with increasing electron-withdrawing character of the substituent attached to the N atom already attached to the anthryl unit. For example, if we compare the absorption behavior of **1**, **3**, and **7** (Figure 5), it is found that  $\lambda_{\text{max}}$  is shifted to 393 nm in **3** in comparison to 349 nm in **7** in dry THF while other peaks remain similar to those found in **1**.

**3.3. Absorption Spectra in the Presence of Transition Metals.** Complexation of **2–8** with transition metal ions causes slight blue-shifts of the transitions with concomitant decrease in the molar extinction coefficients. The blue-shift results from the reduction of charge density over the donor N atom decreasing the charge-transfer character.<sup>26</sup> However, it is difficult to resolve the transitions occurring and the effect of complexation from the absorption spectra due to their complex nature.

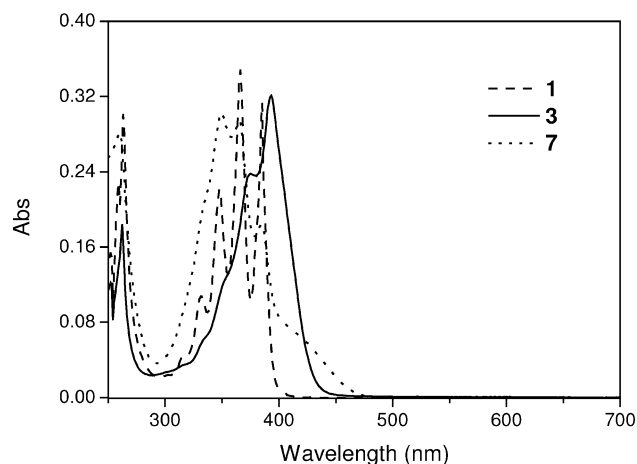


**Figure 5.** Absorption spectra of **1**, **3**, and **7** at  $1 \times 10^{-5}$  M concentration in THF.

Titration of **2** with Cu(II) ion shows a gradual decrease in molar absorptivity ( $\epsilon$ ,  $\text{dm}^3 \text{mol}^{-1} \text{cm}^{-1}$ ) for the peaks at 393 and 373 nm (Figure 6). When no Cu(II) ion is added, the peak at 393 nm ( $\epsilon = 25\,589$ ) is prominent over the one at 373 nm ( $\epsilon = 23\,550$ ). Upon complexation with 1 equiv of Cu(II), the  $\epsilon$  values of the peaks decrease to different extents with the peak at 373 nm ( $\epsilon = 19\,404$ ) dominating over the one at 393 nm ( $\epsilon = 17\,854$ ). Both the peaks show similar molar absorptivity when 0.5 equiv of Cu(II) is added. However, stoichiometry of the complexation cannot be determined due to overlapping ICT and PET transitions. The same is observed for **3** (Figure 6c) and **4**. Moreover, for the simple system **5** (without the anthracene fluorophore), titration with either Zn(II) or Cu(II) shows 1:1 complex formation. The titration curves for the absorption vs metal concentration in acetonitrile are shown in the Figure 7. The ICT transition exhibits a blue-shift with lowering intensity till the addition of 1 equiv of metal; it remains almost constant thereafter.

For **6**, the peak at 351 nm exhibits a blue-shift to the extent of  $\sim 12$  nm upon complexation with Cu(II) while with other metals the shift is slightly less. While **7** shows a slight red-shift, compound **8** shows a blue-shift in the presence of all the transition metals studied. Interestingly, these combined transitions are shifted toward the lower energy region upon complexation with transition metal ions. At the same time, charge-transfer absorption shifts to higher energy upon complexation at the donor end due to a decrease in charge-transfer character that destabilizes the excited-state dipole moment more than that of the ground state. The absorption energy of the charge separated electron-transfer process occurring at the other end of the molecule involving other donor N atom also increases upon complexation as it destabilizes more the  $\text{D}^{+\bullet}-\text{A}^{-\bullet}$  state. When both processes occur at the same time, the destabilization of the charge separated ET state interferes with the charge-transfer transition. Upon complexation, electron density over the donor N atom of the  $\text{D}-\pi-\text{A}$  fragment is more delocalized toward the  $\pi$  system of the electron withdrawing substituent that stabilizes the excited-state dipole moment more than that of the ground state, thus shifting the absorption to lower energy.

**3.4. Emission Studies.** Compound **1** shows a well-resolved emission from the locally excited lowest  $^1(\pi, \pi^*)$  state typical of 9-alkyl substituted<sup>13,27</sup> anthracene. The (0,0) emission band appears at 391 nm in dry THF along with the vibrational structures at 413 and 440 nm. These bands are slightly blue-shifted in acetonitrile medium. The fluorescence quantum yield ( $\phi_F = 0.00216$  in THF) is low due to PET from the donor

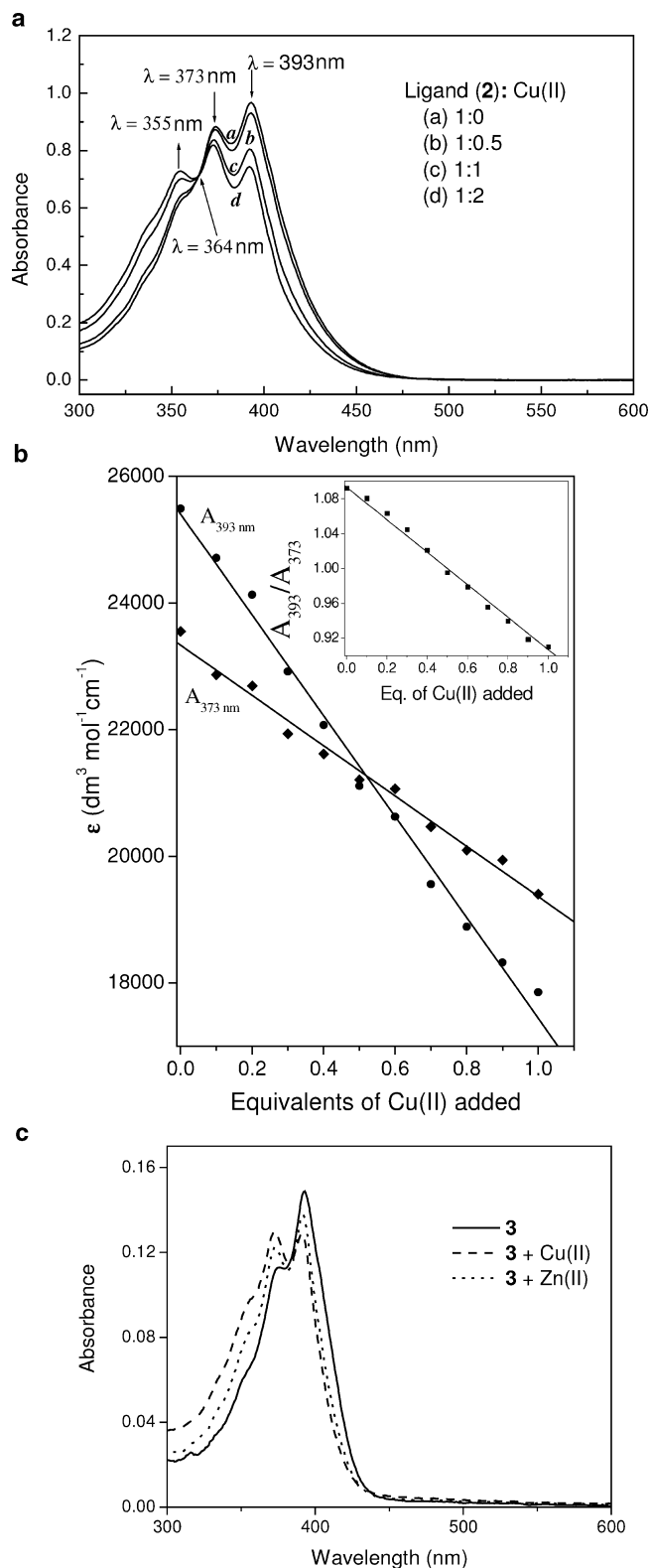


**Figure 6.** (a) Change in absorption spectra of **2** (concentration  $3.9 \times 10^{-5}$  M) upon addition of Cu(II) ion. (b) Plot of  $\epsilon$  vs equivalents of Cu(II) added to **2**. (c) Absorption of **3** (concentration  $0.5 \times 10^{-5}$  M) alone and in the presence of Cu(II) and Zn(II) in THF.

secondary N atom to the anthracene  $\pi$ -system in the excited state. In **2**, **3**, and **4**, the presence of an electron-withdrawing ( $\pi$ -acceptor) group attached to the N atom causes the anthracene emission (Figure 8a) to be slightly red-shifted (3–5 nm) with concomitant appearance of an ICT transition between the N and the  $\pi$ -acceptor. In case of **6**, the emission is red-shifted by 25

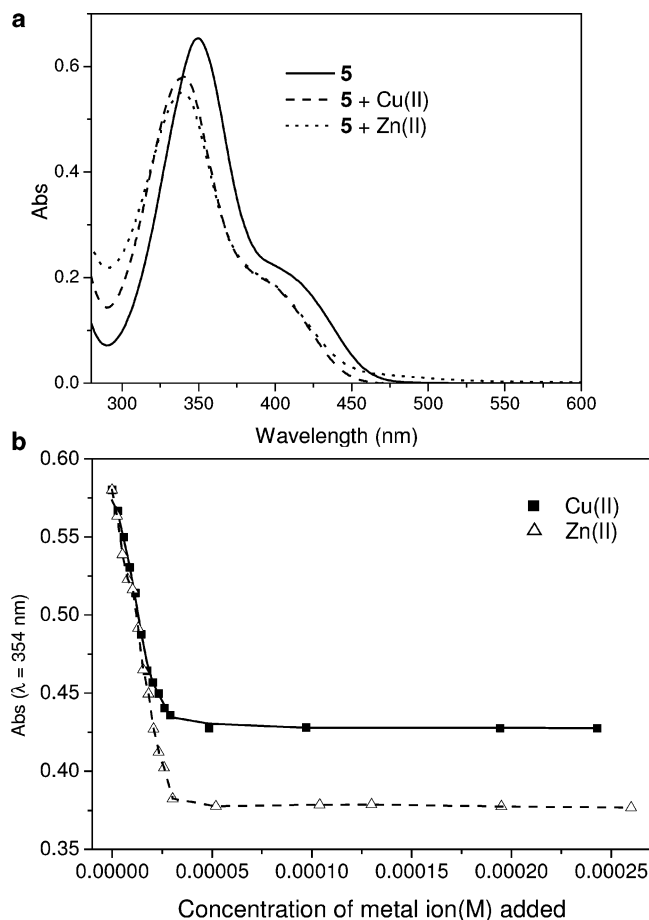


**Figure 7.** (a) Absorption spectra of **5** alone and in the presence of Cu(II), Zn(II) in dry THF at  $3.2 \times 10^{-5}$  M concentration. (b) Change in the absorption of **5** at 354 nm in MeCN upon addition of metal ions at  $3.0 \times 10^{-5}$  M concentration.

nm in comparison to **2**, keeping the emission pattern the same as above but with a slightly different excitation spectrum (Figure 8b). Depending upon the electron-withdrawing nature of the  $\pi$ -acceptor, the ICT transition modulates the PET process to a different extent. More importantly, the fluorescence quantum yields in these compounds are found to be lower compared to that of **1** in THF medium: **2** ( $\phi_F = 0.00043$ ), **3** ( $\phi_F = 0.0015$ ), and **4** ( $\phi_F = 0.0009$ ). Of course, apart from PET, some other processes such as internal bond rotation, quenching due to conformational relaxation<sup>28,29</sup> through modulation of nonradiative processes, competition between simultaneously operative processes, and so on may also be involved. The emission observed in **5** originates from charge-transfer transition<sup>30</sup> involving the N atom and the  $\pi$ -acceptor moiety and is solvatochromic in nature. The emission maximum appears at 363 nm in hexane which is  $\sim 41$  nm red-shifted in DMSO (Figure 9). The increase in Stokes shift with solvent polarity is indicative of a higher dipole moment in the excited state than that in the ground state, which in turn indicates the emission to be an allowed CT transition. The emission quantum yield in nonpolar solvents is low although it is higher in polar solvents (Table 2). Both these are consistent<sup>4b,31</sup> with the fact that the excited ICT states are effectively stabilized in polar media.

Absorption and emission spectral studies of all the systems except **5** were also carried out in different solvents<sup>22</sup> to probe the effect of solvent polarity on these transitions. The spectral data indicate that for compounds with an attached  $\pi$ -acceptor group, the relative intensities of the (0,0) and the vibrational

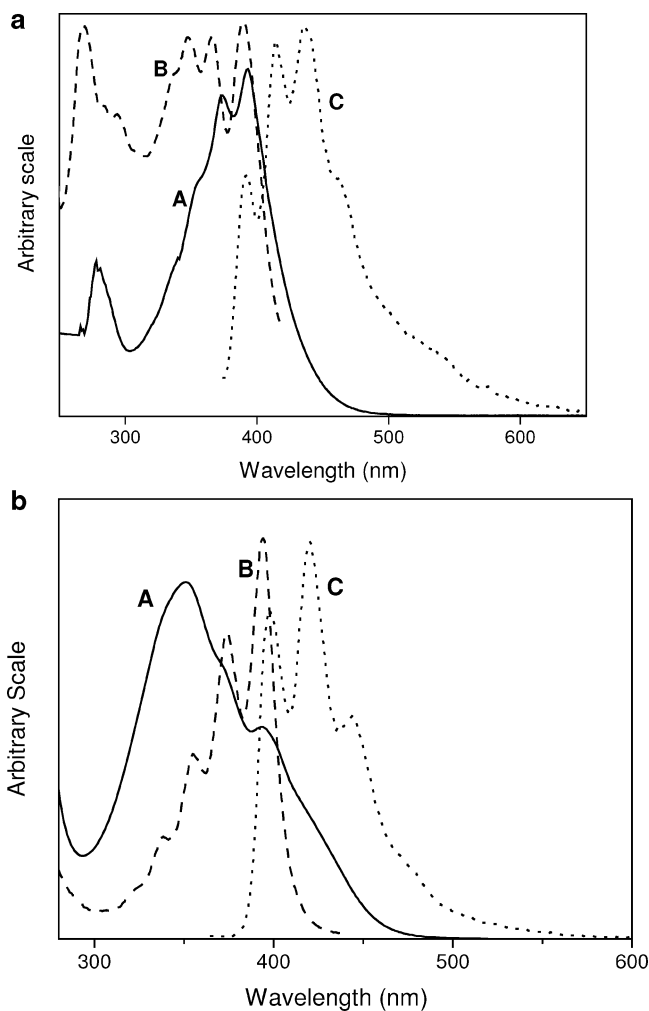


**Figure 8.** Absorption (solid), excitation (dashed), and emission spectra (dotted) of **2** (a) and **6** (b) in dry THF. All the spectra were plotted in arbitrary scale for comparison.

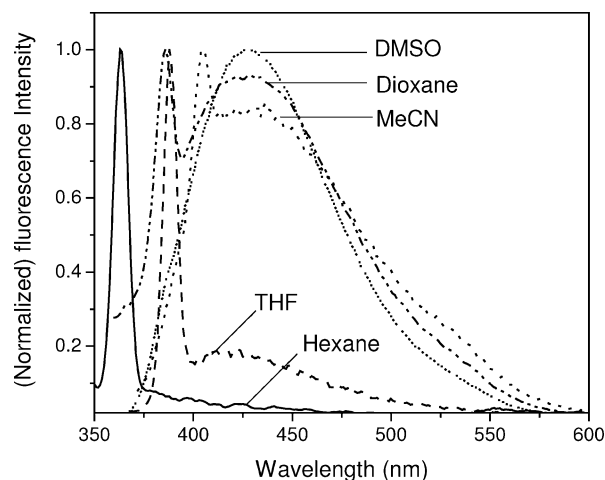


**Figure 9.** Emission spectra (normalized) of **5** in various solvents.

bands change significantly although the absorption or emission spectral positions remain unchanged with solvent polarity. Charge transfer states are effectively stabilized in polar media due to charge-dipole interaction of the polarized excited state with the solvent. Therefore, polar solvents will lead to a greater Stokes' shift. However, positions of the absorption and emission peaks do not vary significantly in **2–4** with solvent polarity. The observed alteration in the vibrational structures of the

**TABLE 2: Absorption, Emission, and Fluorescence Quantum Yield of **5** in Various Solvents**

solvent	$\lambda_{\text{abs}}$ , nm ( $\epsilon$ , dm <sup>3</sup> mol <sup>-1</sup> cm <sup>-1</sup> )	$\lambda_{\text{em}}^{\text{max}}$ (nm)	$\phi_{\text{F}}$
hexane	330 (12110); 387 (3780)	363	0.00086
cyclohexane	334 (7864); 388 (2396)	368	0.00083
1,4-dioxane	348 (4794); 416 (1354)	385	0.00192
toluene	347 (20580); 415 (4958)	385	0.00259
chloroform	350 (24472); 418 (6917)	389	0.00018
dichloromethane	352 (21135); 423 (7247)	393	0.00222
ethyl acetate	347 (22033); 420 (5558)	384	0.00539
THF	352 (19778); 414 (4140)	389	0.00792
acetone	352 (19909); 422 (5709)	401	0.00943
methanol	350 (15729); 418 (4674)	389	0.01824
ethanol	348 (25121); 417 (7410)	394	0.00248
acetonitrile	352 (19660); 424 (5675)	399	0.00546
dimethyl formamide	358 (21600); 428 (6955)	406	0.01845
dimethyl sulfoxide	363 (20864); 431 (6434)	417	0.02991

anthracene bands may be due to some spatial  $\pi$  electronic interaction between the  $\pi$ -acceptor and the anthracene moieties. The fluorescence quantum yield (Table 3) of **1** decreases with an increase in polarity of the solvent as PET is enhanced in polar medium<sup>32</sup> due to charge-dipole interaction. In contrast, the  $\phi_{\text{F}}$  in **2–4** is found to be larger in solvents with high polarity due to higher charge-transfer character and less electron density in the donor N making the PET process less probable.

The emission bands in **7** and **8** are slightly blue-shifted (~5 nm) compared to that for **1**. The (0,0) band appears at 386 nm in **7** and **8** and the  $\phi_{\text{F}}$  for **7** and **8** in THF are found to be 0.00044 and 0.00197, respectively. A comparison of the  $\phi_{\text{F}}$  of **7** with that of **1** and of **8** with that of **2** indicates that the electron-donating *N,N*-dimethylamino group in place of the electron-withdrawing 2,4-dinitrobenzene at the opposite end of the fluorophore in the amino-alkyl-amino chain leads to comparatively lower quantum yields. It follows, therefore, that a long-range PET might be operative concurrently from the N of the dimethylamino moiety in **1–4** to the anthracene group. Thus, it is evident that the occurrence of the ICT process affects the PET in these systems. However, the fluorophore and the receptor distances and the orientation between them also contribute in the overall PET process.

### 3.5. Emission in the Presence of Transition Metal Ions.

With a transition metal ion as input, the emission intensity increases in some cases depending on the overall architecture of the system (Table 4). In cases where enhancement is observed, the (0,0) band position does not show any noticeable shift due to minimum interaction between a metal ion and the fluorophore. However, a different intensity ratio of the (0,0) and the first vibrational bands is observed in each case compared to the metal-free state. In **1**, addition of Zn(II) gives an enhancement factor of 122 with respect to the metal-free state, while other transition metals do not show any significant enhancement owing to their quenching nature. Fluorescence titrations of **1** with Zn(II) in both THF and acetonitrile show that **1** forms a 2:1 complex (Figure 10).

Significantly, attachment of a 2,4-dinitrobenzene group to **1** (to get **2**) drastically alters its emission characteristics. Compound **2** shows high specificity for Cu(II) among the transition metal ions studied with the enhancement showing at least 100-fold increase with respect to metal-free **2** in acetonitrile as well as in THF (Table 4, Figure 11). For other transition metal ions including Zn(II), the enhancement factor is below 10. Such a drastic change in the emission characteristics and selectivity upon modification of a receptor in “fluorophore-spacer-receptor” systems is unprecedented. This could be due to strongest interaction of Cu(II) in comparison to other metal ions,

**TABLE 3: Absorption and Emission Maxima and  $\phi_{\text{F}}$  of the Compounds in Various Solvents<sup>a</sup>**

fluorophoric systems	solvents	$\lambda_{\text{max}}^{\text{abs}}$ , nm ( $\epsilon$ , dm <sup>3</sup> mol <sup>-1</sup> cm <sup>-1</sup> )	$\lambda_{\text{max}}^{\text{em}}$ , nm	$\phi_{\text{F}}$	
<b>1</b>	cyclohexane	368 (9249)	388	0.07693	
	CHCl <sub>3</sub>	367 (17070)	417	0.03153	
	THF	366 (9767)	413	0.00216	
	MeOH	364 (18228)	388	0.01241	
	acetone	365 (18072)	387	0.02340	
	EtOH	366 (17212)	410	0.01793	
	MeCN	365 (10136)	389	0.00137	
	DMF	363 (15992)	414	0.00064	
	<b>2</b>	cyclohexane	372 (19108)	391	0.0001
		DCM	394 (21815)	393	0.0057
CHCl <sub>3</sub>		393 (30391)	394	0.0009	
THF		394 (25489)	394	0.0004	
MeOH		391 (19156)	392	0.0093	
acetone		392 (23352)	393	0.0043	
EtOH		394 (25671)	394	0.0087	
MeCN		392 (25358)	394	0.0185	
DMF		395 (25949)	396	0.0293	
DMSO		397 (26674)	398	0.0426	
<b>3</b>	cyclohexane	390 (23856)	411	0.0008	
	CHCl <sub>3</sub>	395 (31546)	415	0.0272	
	THF	393 (32085)	414	0.0015	
	MeOH	391 (28595)	389	0.06057	
	acetone	393 (32862)	387	0.0220	
	EtOH	391 (28008)	410	0.02298	
	MeCN	394 (31293)	389	0.0143	
	DMF	398 (32682)	389	0.0411	
	<b>4</b>	cyclohexane	389 (22176)	417	0.0003
		CHCl <sub>3</sub>	393 (30554)	416	0.0050
THF		371 (30385)	416	0.0009	
MeOH		370 (30461)	388	0.00453	
acetone		390 (33515)	388	0.00324	
EtOH		371 (33754)	388	0.01148	
MeCN		390 (28740)	389	0.03832	
DMF		391 (33816)	415	0.03985	
<b>6</b>		cyclohexane	340 (n. d.)	416	
		CHCl <sub>3</sub>	342 (n. d.)	417	
	THF	351(39594)	419	0.0052	
	MeOH	341(40214)	389	0.0387	
	acetone	352(41630)	387	0.0012	
	EtOH	341(38833)	388	0.01364	
	MeCN	347(43890)	389	0.00153	
	DMF	340(34045)	424	0.00067	
	<b>7</b>	cyclohexane	368(19774)	418	0.0003
		CHCl <sub>3</sub>	350(23319)	417	0.0061
THF		349(30229)	418	0.00044	
MeOH		348(29315)	389	0.0334	
acetone		364(25616)	387	0.0024	
EtOH		364(31715)	388	0.0363	
MeCN		364(29568)	388	0.00168	
DMF		363(28715)	412	0.00369	
<b>8</b>		cyclohexane	355 (n. d.)	419	
		CHCl <sub>3</sub>	355(43148)	417	0.0029
	THF	372(36411)	416	0.00197	
	MeOH	369(41824)	389	0.0153	
	acetone	371(34433)	388	0.0037	
	EtOH	368(39960)	388	0.00796	
	MeCN	371(45008)	389	0.00262	
	DMF	267(41092)	409	0.00198	

<sup>a</sup> Experimental conditions: concentration of free ligand,  $\sim 1 \times 10^{-6}$  M; excitation band-pass, 5 nm; emission band-pass, 5 nm; temperature, 293 K. All the samples were excited at  $\lambda_{\text{ex}} = 350$  nm for comparison.  $\phi_{\text{F}}$  is calculated by comparison of corrected spectrum with that of anthracene ( $\phi_{\text{F}} = 0.297$ ) taking the area under the total emission. The error in  $\phi_{\text{F}}$  is within  $\pm 10\%$  in each case.

with the lone-pair on N2 in **2** overriding its quenching nature. All attempts to isolate single crystals of the Cu(II) complex of **2** remained unsuccessful. Fluorescence titrations reveal a 1:1 complex formation with the metal (Figure 11c). Further addition of Cu(II) in high concentration (100 times) results in the

**TABLE 4: Fluorescence Quantum Yield<sup>a</sup> and Fluorescence Enhancement (FE) of the Fluorophoric Systems in the Presence of Various Transition Metal Ion Input**

fluorophoric system	medium	ionic input	quantum yield ( $\phi_F$ )	fluorescence enhancement		
1	THF	Nil	0.00216	1 (standard)		
		Mn(II)	0.0281	13		
		Fe(II)	0.00864	4		
		Co(II)	0.00648	3		
		Ni(II)	0.00644	3		
		Cu(II)	0.00236	1		
		Zn(II)	0.2645	122		
		Cd(II)	0.00239	1		
		H <sup>+</sup>	0.0756	35		
		Acetonitrile	Nil	0.00137	1 (standard)	
			Zn(II)	0.14473	106	
2	THF	Nil	0.00043	1 (standard)		
		Mn(II)	0.00344	9		
		Fe(II)	0.00086	2		
		Co(II)	0.00433	10		
		Ni(II)	0.00129	3		
		Cu(II)	0.04644	108		
		Zn(II)	0.00131	3		
		Cd(II)	0.00044	1		
		H <sup>+</sup>	0.00089	2		
		3	THF	Nil	0.0015	1 (standard)
				Mn(II)	0.0210	14
Fe(II)	0.0163			11		
Co(II)	0.0555			37		
Ni(II)	0.0468			31		
Cu(II)	0.0315			21		
Zn(II)	0.0153			10		
Cd(II)	0.0075			5		
H <sup>+</sup>	0.0094			6		
4	THF			Nil	0.0009	1 (standard)
				Mn(II)	0.0371	41
		Fe(II)	0.0036	4		
		Co(II)	0.0135	15		
		Ni(II)	0.0324	36		
		Cu(II)	0.0252	28		
		Zn(II)	0.0054	6		
		Cd(II)	0.0073	8		
		H <sup>+</sup>	0.0144	16		
		6	THF	Nil	0.0052	1 (standard)
				Mn(II)	0.1599	31
Fe(II)	0.0565			11		
Co(II)	0.1698			33		
Ni(II)	0.1784			34		
Cu(II)	0.2468			48		
Zn(II)	0.1970			38		
Cd(II)	0.0081			1.6		
H <sup>+</sup>	0.0063			1.2		
7	THF			Nil	0.00044	1 (standard)
				Mn(II)	0.00098	2
		Fe(II)	0.00137	3		
		Co(II)	0.04310	99		
		Ni(II)	0.00609	14		
		Cu(II)	0.00134	3		
		Zn(II)	0.00388	8		
		Cd(II)	0.00049	1		
		H <sup>+</sup>	0.00534	11		
		8	THF	Nil	0.00197	1 (standard)
				Mn(II)	0.02174	11
Fe(II)	0.26604			132		
Co(II)	0.05516			28		
Ni(II)	0.00592			3		
Cu(II)	0.08028			41		
Zn(II)	0.01379			7		
Cd(II)	0.00788			4		
H <sup>+</sup>	0.00594			3		

<sup>a</sup> Experimental conditions: concentration of free ligand,  $10^{-6}$  M; concentration of the metals,  $\sim 10^{-4}$ – $10^{-5}$  M; excitation band-pass, 5 nm; emission band-pass, 5 nm; temperature, 293 K. All the samples were excited at  $\lambda_{\text{max}}^{\text{abs}}$  of the corresponding ligands.  $\phi_{\text{FT}}$  is calculated by comparison of the corrected spectrum with that of anthracene ( $\phi_{\text{FT}} = 0.297$ ) taking the area under the total emission. The error in  $\phi_{\text{FT}}$  is within  $\pm 10\%$  in each case.

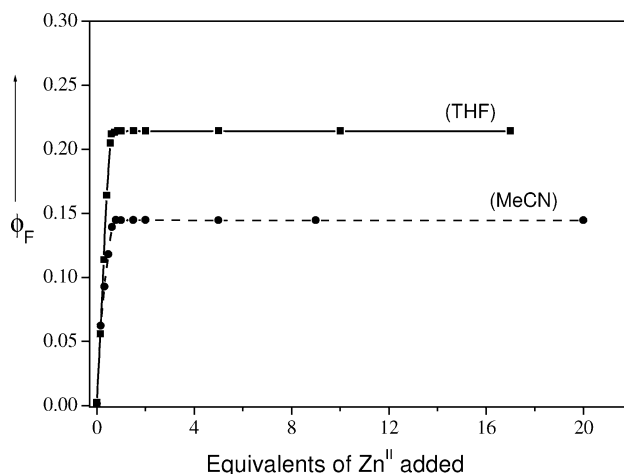


**Figure 10.** Fluorescence quantum yield ( $\phi_F$ ) of **1** upon Zn(II) addition in THF (concentration  $1.7 \times 10^{-6}$  M) and MeCN (concentration  $2.0 \times 10^{-6}$  M).

decrease of fluorescence intensity as expected from a quenching metal ion.<sup>15</sup> Compounds **3** and **4** do not show any specificity for any metal ion (Table 4). Among the metal ions studied, Co(II), Ni(II), and Cu(II) show appreciable fluorescence recovery. Compound **6** shows  $\sim 50$ -fold increase in fluorescence quantum yield with Cu(II) in dry THF. Interestingly, a structurally similar compound without the two 2,4-dinitrobenzene groups was reported<sup>33</sup> to exhibit 1000-fold fluorescence enhancement with Zn(II) while at the same time, other transition metals were not reported to show any enhancement. Thus, attachment of two electron-withdrawing groups has led to tuning of the binding property of the receptor, which in turn modulates the sensitivity and selectivity of the fluorophoric system. The selectivity in binding is also apparent in **7** where the fluorophore and the electron-withdrawing groups are situated at either end of the “alkyl–amino–alkyl” framework. This compound shows Co(II) selectivity with an enhancement factor of 100 with this metal while other metals do not give enhancement more than 10 times. Although compound **8** does not show any specificity toward any transition metal ions, the fluorescence recovery is maximum with Fe(II). The nature of the fluorescence titration curve of **8** with Fe(II) and Cu(II) in dry THF indicates that it forms a 1:1 complex with either metal (Figure 11d). A sigmoidal titration curve is observed for **8** with Fe(II), which may be due to a change in the binding pattern of Fe(II) in the complex with its concentration in the solution. A similar shape of the titration curves has been observed by others in different systems.<sup>34</sup>

**3.6. Complex Stability Constants.** For the cases where a substantial change in absorbance or fluorescence intensities are observed in the concentration range  $\sim 10^{-5}$ – $10^{-6}$  M, the complex stability constant ( $K_s$ ) can be determined.<sup>30,35</sup> In most of the cases, therefore,  $K_s$  could not be determined with proper accuracy as an increase in fluorescence/absorbance intensity is not substantial. For the complexation of **1** with Zn(II), a 2:1 (ligand:metal) complexation is observed, which is in agreement with the plot of fluorescence quantum yield of **1** as a function of Zn(II) concentration (Figures 10 and 11a). The  $K_s$  value ( $4.2 \times 10^4 \text{ M}^{-1}$ ) for this metal could be obtained with other implicit functions.<sup>16a,8b</sup> For **2**, the  $K_s$  with Cu(II) is found to be  $4.42 \times 10^4 \text{ M}^{-1}$  from fluorescence data while from the absorption spectral data it is found to be  $3.78 \times 10^4 \text{ M}^{-1}$  at  $\lambda = 393 \text{ nm}$  and  $2.39 \times 10^4 \text{ M}^{-1}$  at  $\lambda = 373 \text{ nm}$ . For system **5**, which does not incorporate the anthryl subunit, the  $K_s$  determined from absorbance spectral data at  $\lambda = 354 \text{ nm}$  affords for Cu(II) and

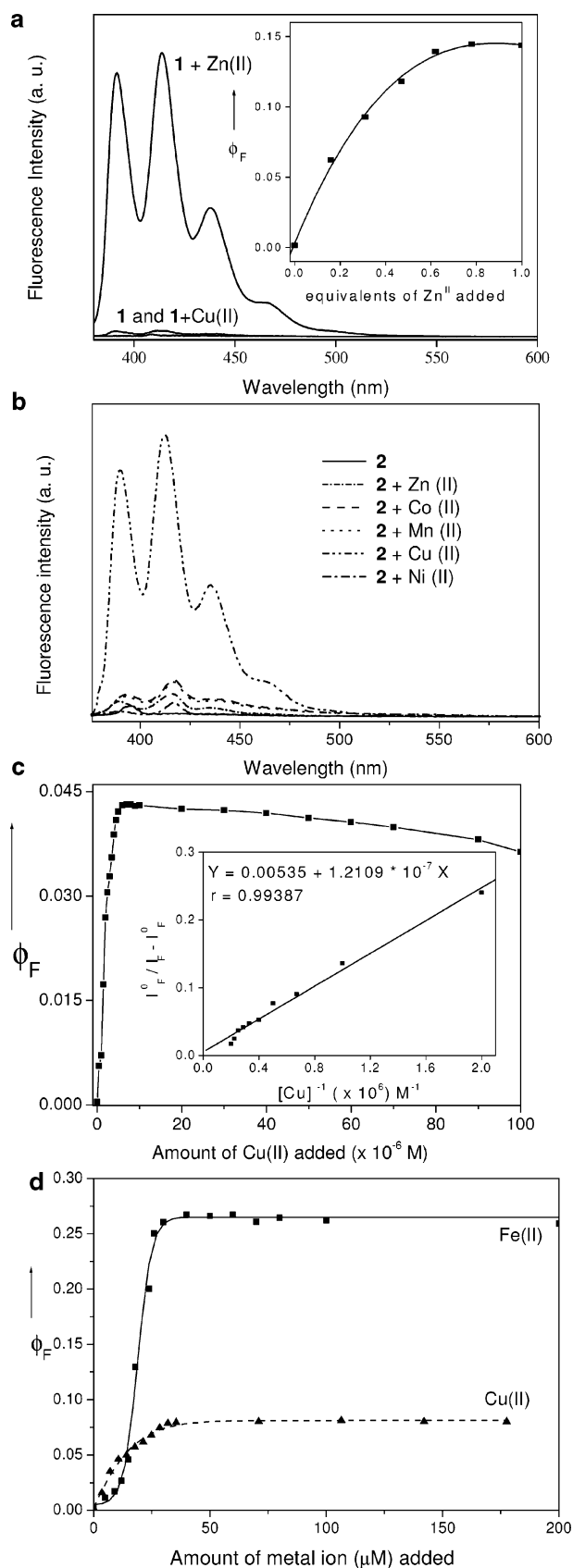


**Figure 11.** Fluorescence spectra of (a) **1** alone and in the presence of Cu(II) and Zn(II). Plot of fluorescence quantum yield vs equivalents of Zn(II) added (inset). (b) **2** alone and in the presence of metal ions. (c) Plot of fluorescence quantum yield of **2** at  $5 \times 10^{-6}$  M concentration vs amount of Cu(II) added in dry THF. Plot of  $I_F^0 / (I_F - I_F^0)$  as a function of  $[Cu(II)]^{-1}$  added (inset). (d) Plot of the fluorescence quantum yield of **8** at  $2.5 \times 10^{-5}$  M concentration vs the amount of metal ion added in dry THF.

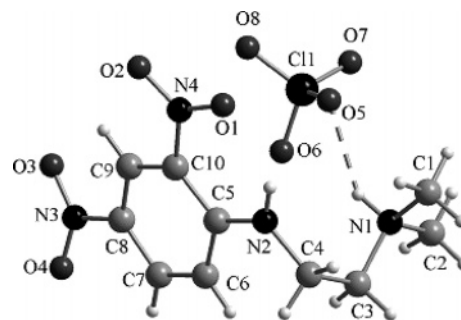


**Figure 12.** Perspective views of the X-ray structures of **5H<sup>+</sup>** showing the atom numbering scheme.

Zn(II) respectively  $4.86 \times 10^4$  and  $5.78 \times 10^4$  M<sup>-1</sup>. Fluorescence data show that in case of **7**, the  $K_s$  with Co(II) yields  $5.11 \times 10^4$  M<sup>-1</sup> while for **8** the  $K_s$  values are  $5.73 \times 10^3$  and  $3.86 \times 10^3$  M<sup>-1</sup> respectively with Fe(II) and Cu(II). Although the data on complex stability constants are not complete, it is found that in cases where substantial fluorescence increases are observed upon addition of a metal salt, the complex stability constants are in the order of  $10^4$  M<sup>-1</sup> which are very similar to those with other systems reported in the literature.<sup>15,36</sup> However, the stability constants determined from the fluorescence data can be taken as the lower limit. The comparatively lower value of  $K_s$  in the case of **8** may be attributed to the lower electron density available at the receptor moiety for metal complexation due to the presence of electron withdrawing 2,4-dinitrobenzene groups attached to both the N atoms of the receptor (Figure 1).

**3.7. Emission in the Presence of Protons.** Hydrated metal perchlorate and nitrate salts can generate protons in organic solvents. These protons can engage the lone pair of nitrogens causing fluorescence enhancement by effectively blocking the PET. To verify that the fluorescence enhancement is due to the metal ion and not because of protonation, certain controlled experiments<sup>12a,4b</sup> were carried out. In the metal free state, the  $\phi_{FT}$  does not change or increases by a negligible amount on changing the solvent from dry THF to aqueous THF (THF:H<sub>2</sub>O 9:1 v/v). Moreover, different metal ions give different extents of enhancement. If the proton generation in the medium by the metal salts were to be responsible, then the extent of enhancement should have been almost the same in all cases.

In dry or aqueous THF medium, the fluorescence enhances by a small factor (1–16 fold) in the presence of HClO<sub>4</sub> ( $1 \times 10^{-3}$  M) for all the systems except **1**, where ~35-fold enhancement is observed. In all the systems except **1**, the basic N atom of the *N,N*-dimethylamino end preferentially becomes protonated, not the donor N atom attached to the electron-withdrawing group and the fluorophore. Reduction of charge density due to attachment of electron-withdrawing groups creates an acidic environment over the donor N atom and thus becomes difficult for protonation. This is evidenced from the single-crystal structure of protonated **5** (Figure 12), which was crystallized under acidic conditions.

In this protonated structure, N1 atoms were protonated and H-bonded to the anion whereas N2 atoms remain unprotonated. However, a substantial fluorescence enhancement is observed upon protonation in **1** as both the donor atoms become bound to proton, which effectively blocks the PET process.

**3.8. AM1 Calculations.** The structure of a fluorophoric system provides vital information toward the thermodynamics of metal binding, in determining the feasibility of the operative processes, and so on. A slight modification of the system can perturb<sup>36</sup> its photophysical property significantly. In the modulation of PET, the distance between two nitrogen

**TABLE 5: Selected Geometrical Parameters for All the Fluorophoric Systems**

fluorophoric systems	$\Sigma N(2)$ angle (deg)	$\Sigma N(1)$ angle (deg)	$\mu_g$ (D)	$r_{N(1)-N(2)}$ (Å)	torsion angle, $\psi$ (deg) <sup>a</sup>
1	334.17	338.18	0.41	3.767	
2	338.87	339.51	4.96	3.779	34.33 <sup>b</sup>
3	345.47	339.25	5.54	3.773	16.91 <sup>b</sup>
4	358.35	337.83	6.97	3.733	34.42 <sup>b</sup>
5	359.99	339.68	8.58	3.747	
6	359.48	338.63	7.12	3.762	-72.02 <sup>b</sup>
7	338.71	359.59	6.98	3.071	52.38 <sup>c</sup>
8	342.89	356.05	11.57	3.035	18.15 <sup>b</sup> /45.68 <sup>c</sup>

<sup>a</sup> Improper torsion angle between anthracene and phenyl ring. <sup>b</sup> When both units are attached to the same N(2) atom. <sup>c</sup> When both units are attached to two different amino ends.

atoms N(1) - -N(2) of the amino–alkyl–amino receptor framework as well as the position of the electron-withdrawing group play crucial roles via modulation of the extent of orbital overlap.<sup>37</sup> Crystal structures of the molecules provide information in the solid state that is driven by packing forces. To complement the solid-state structures of the molecules, geometrical optimization for the systems was carried out by employing the semiempirical AM1 method (gradient <0.001, Hyperchem version 7.0, Hypercube Inc). The atom numbering schemes as in the X-ray crystal structures were retained here. The sum of the angles around the nitrogen atoms of the amino–alkyl–amino unit, the N(1) - -N(2) distance, the ground-state dipole moment, and the twist angle between the  $\pi$  electronic rings of all the systems are collected in the Table 5.

The sum of the angles around the N(2) atom suggests that its degree of pyramidalization is low. However, it is almost planar in **5**. The sum of the angles around N(1) points to a nonplanar geometry in **1**, **2**, **3**, **4**, **5**, and **6** similar to that of a sp<sup>3</sup> hybridized pyramidal nitrogen, whereas in **7** and **8** it is planar. The energy of the charge-transfer state is much influenced by the strength of the electron donor and acceptor moieties. The ground-state dipole moment of **1** is significantly lower compared to other systems. Attachment of electron-withdrawing group(s) increases the ground-state dipole moment favoring charge separation. The ground-state dipole moment is much higher in **8** compared to other compounds in the series. Consequently, the molar extinction coefficient of **8** is found to be higher than in other systems. This indicates a favorable N(2) geometry for charge separation in **8**. The improper twist angle between the anthracenyl and the phenyl ring, which quantifies the  $\pi$  electronic interaction between the ring systems, is consistent with the spectral responses of the molecules. The N(1) - -N(2) distance in the amino–alkyl–amino framework varies with the nature of the substituents on the N(1) atom. It is found to be shorter when substituted with an electron-withdrawing group compared to the molecules substituted with two methyl groups to this distal end. Apart from determining the PET rate, the N(1) - -N(2) distance also contributes toward fluorescence recovery upon selective metal ion coordination. A larger  $r_{N(1)-N(2)}$  distance will favor binding a smaller cation.<sup>38</sup> The  $r_{N(1)-N(2)}$  distance is maximum in **2** that shows selectivity for the Cu(II) ion which has a comparatively smaller ionic radius among the metal ions probed. However, single-crystal X-ray structures of the metal complexes are necessary before a conclusion can be put forward regarding selectivity. All attempts to obtain X-ray quality crystals of the metal complexes remained unsuccessful.

## 4. Conclusion

We have shown here that simple multicomponent systems in the format fluorophore–spacer–receptor can be designed through the modular approach. Attachment of electron-withdrawing group(s) in these systems profoundly alters their photophysical properties. The modular design principles can be conveniently applied to tune the binding characteristics of the receptor. The extent of change in the photophysical properties critically depends on the spatial relationship of different moieties with respect to each other as several processes operate simultaneously. It is of interest to point out here that even when a quenching paramagnetic transition metal ion is capable of interacting with the fluorophore, it is possible to exhibit fluorescence enhancement. Although the exact reason for the enhancement is still not clear, it suggests that for fluorescence enhancement with similar systems, the quantum yield should be very low in the absence of a metal ion as input. Selectivity in the binding of a metal ion to the receptor with concomitant enhancement of fluorescence can be brought about by tuning the overall architecture of the system. If the bite angle is optimum for a particular metal ion, then higher selectivity can be achieved.<sup>38</sup> This specific sensing ability of a fluorescent signaling system is of enormous importance in biomedical research. We are presently working on other acyclic receptors with wide structural variations as well as different orientations with respect to the fluorophore to understand how paramagnetic transition metal ions, which are known quenchers, can cause fluorescence enhancement.

**Acknowledgment.** Financial support for this work from the Department of Science and Technology, New Delhi is gratefully acknowledged. B.P.B. thanks CSIR, New Delhi for a Senior Research Fellowship.

**Supporting Information Available:** Crystallographic data (CIF) for **2**, **3**, **4**, **5**, **7**, **8**, and **5H**, and characterization of the ligands **1–8** including FABMS, <sup>13</sup>C NMR, <sup>1</sup>H NMR, UV–vis spectral data, and fluorescence spectra. This material is available free of charge via the Internet at <http://pubs.acs.org>.

## References and Notes

- (1) (a) *Fluorescent Chemosensors of Ion and Molecule Recognition*; Czarnik, A. W., Ed.; ACS Symp. Ser. 538; American Chemical Society: Washington, DC, 1993. (b) Fabbrizzi, L.; Poggi, A. *Chem. Soc. Rev.* **1995**, *25*, 197. (c) Valeur, B. In *Topics in Fluorescence Spectroscopy*; Lakowicz, J. R., Ed.; Plenum Press: New York, 1994; Vol. IV. (d) Czarnik, A. W. *Acc. Chem. Res.* **1994**, *27*, 302.
- (2) (a) Wolfram, J.; Sauer, M. In *Applied Fluorescence in Chemistry, Biology and Medicine*; Rettig, W., Strehmel, B., Schrader, S., Seifert, H., Eds.; Springer-Verlag: Berlin, Germany, 1999. (b) Rurack, K. *Spectrochim. Acta A* **2001**, *57*, 2161.
- (3) de Silva, A. P.; Gunaratne, H. Q. N.; Gunnlaugsson, T.; Huxley, A. J. M.; McCoy, C. P.; Radmacher, J. T.; Rice, T. E. *Chem. Rev.* **1997**, *97*, 1515.
- (4) (a) Szurdoki, F.; Ren, D.; Walt, D. R. *Anal. Chem.* **2000**, *72*, 5250. (b) Ramachandram, B.; Saroja, G.; Sankaran, N. B.; Samanta, A. *J. Phys. Chem. B* **2000**, *104*, 11824. (c) Balzani, V.; Ceroni, P.; Gestermann, S.; Kaufmann, C.; Gorka, M.; Vögtle, F. *Chem. Commun.* **2000**, 853. (d) Klein, G.; Kaufmann, D.; Schürch, S.; Reymond, J.-L. *Chem. Commun.* **2001**, 561. (e) Reany, O.; Gunnlaugsson, T.; Parker, D. *Chem. Commun.* **2000**, 473.
- (5) de Silva, A. P.; McClenaghan, N. D.; McCoy, C. P. In *Electron Transfer in Chemistry*; Balzani, V., Ed.; Wiley-VCH: Weinheim, Germany, 2000; Vol. 5.
- (6) (a) Bard, A. J. *Chem. Eng. News* **1999**, Sept 6, 5. (b) *Digital Computer Electronics*, 3rd ed.; Malvino, A. P., Brown, J. A., Eds.; Glencoe: Lake Forest, NY, 1993. (c) Haarer, D. *Angew. Chem., Int. Ed. Engl. Adv. Mater.* **1989**, *28*, 11, 1544. (d) de Silva, A. P.; McClenaghan, N. D.; McCoy, C. P. In *Molecular Electronics*; Feringa, B. L., Ed.; Wiley-VCH: Weinheim, Germany, 2001.

- (7) (a) de Silva, A. P.; Gunaratne, H. Q. N.; McCoy, C. P. *Nature* **1993**, *364*, 42. (b) de Silva, A. P.; Gunaratne, H. Q. N.; McCoy, C. P. *J. Am. Chem. Soc.* **1997**, *119*, 7891. (c) Credi, A.; Balzani, V.; Langford, S. J.; Stoddart, J. F. *J. Am. Chem. Soc.* **1997**, *119*, 2679. (d) de Silva, A. P.; Dixon, I. M.; Gunaratne, H. Q. N.; Gunnlaugsson, T.; Maxwell, P. R. S.; Rice, T. E. *J. Am. Chem. Soc.* **1999**, *121*, 1393. (e) Brown, G. J.; de Silva, A. P.; Pagliari, S. *Chem. Commun.* **2002**, 2461.
- (8) (a) Ji, H.-F.; Dabestani, R.; Brown, G. M. *J. Am. Chem. Soc.* **2000**, *122*, 9306. (b) Ruarck, K.; Kollmannsberger, M.; Resch-Genger, U.; Daub, J. *J. Am. Chem. Soc.* **2000**, *122*, 968. (c) Remacle, F.; Speiser, S.; Levine, R. D. *J. Phys. Chem. B* **2001**, *105*, 5589. (d) Raymo, F. M.; Giordani, S. *J. Am. Chem. Soc.* **2002**, *124*, 2004. (e) Raymo, F. M. *Adv. Mater.* **2002**, *14*, 401.
- (9) Kavarnos, G. J. *Fundamentals of Photoinduced Electron Transfer*; VCH: Weinheim, Germany, 1993.
- (10) (a) Kemlo, J. A.; Shepard, T. M. *Chem. Phys. Lett.* **1977**, *47*, 158. (b) Varnes, A. W.; Dodson, R. B.; Wehry, E. L. *J. Am. Chem. Soc.* **1972**, *94*, 946.
- (11) (a) Rurack, K.; Resch-Genger, U. *Chem. Soc. Rev.* **2002**, *31*, 116. (b) Bharadwaj, P. K. *Prog. Inorg. Chem.* **2003**, *51*, 251.
- (12) (a) Ghosh, P.; Bharadwaj, P. K.; Roy, J.; Ghosh, S. *J. Am. Chem. Soc.* **1997**, *119*, 11903. (b) Das, G.; Bharadwaj, P. K.; Roy, M. B.; Ghosh, S. *J. Photochem. Photobiol. A* **2000**, *135*, 7. (c) Das, G.; Bharadwaj, P. K.; Roy, M. B.; Ghosh, S. *Chem. Phys.* **2002**, *277*, 145. (d) Bag, B.; Bharadwaj, P. K. *J. Lumin.* **2004**, *110*, 85.
- (13) Birks, J. B. *Photophysics of Aromatic Molecules*; Wiley-Interscience, New York, 1970.
- (14) (a) Uchiyama, S.; Matsumura, Y.; de Silva, A. P.; Iwai, K. *Anal. Chem.* **2003**, *75*, 5926. (b) Onoda, M.; Uchiyama, S.; Santa, T.; Imai, K. *Anal. Chem.* **2002**, *74*, 4089.
- (15) Fery-Forgues, S.; Le Bries, M.-T.; Guetté, J.-P.; Valeur, B. *J. Phys. Chem.* **1988**, *92*, 6233.
- (16) (a) Bourson, J.; Pouget, J.; Valeur, B. *J. Phys. Chem.* **1993**, *97*, 4552. (b) Banthia, S.; Samanta, A. *J. Phys. Chem. B* **2002**, *106*, 5572.
- (17) Armarego, W. L. F.; Perrin, D. D. *Purification of Laboratory Chemicals*, 3rd ed.; Pergamon Press: Oxford, UK, 1988.
- (18) Miller, M. W.; Amidon, R. W.; Tawney, P. O. *J. Am. Chem. Soc.* **1955**, *77*, 2845.
- (19) *International Tables for X-ray Crystallography*; Kynoch Press: Birmingham, England, 1994; Vol. IV.
- (20) Altomare, A.; Burla, M. C.; Camalli, M.; Casciarano, G. L.; Giacovazzo, C.; Guagliardi, A.; Moliterni, A. G. G.; Polidori, G.; Spagna, R. *J. Appl. Crystallogr.* **1999**, *32*, 115.
- (21) Sheldrick, G. M. *SHELXL-97*, Program for Crystal Structure Refinement; University of Göttingen: Göttingen, Germany, 1997.
- (22) See the Supporting Information.
- (23) Sankaran, N. B.; Das, A.; Samanta, A. *Chem. Phys. Lett.* **2002**, *351*, 61.
- (24) Mukhopadhyay, P.; Bharadwaj, P. K.; Krishnan, A.; Das, P. K. *J. Mater. Chem.* **2002**, *12*, 2786.
- (25) Absorption of nitro-substituted aniline is highly solvatochromic in nature, for example: (a) Millefiori, S.; Favini, G.; Millefiori, A.; Grasso, D. *Spectrochim. Acta* **1975**, *33*, 21. (b) Kovalenko, S. A.; Schanz, R.; Farztdinov, V. M.; Hennig, H.; Ernsting, N. P. *Chem. Phys. Lett.* **2000**, *323*, 312.
- (26) (a) Valeur, B.; Leray, I. *Coord. Chem. Rev.* **2000**, *3*, 205. (b) Martin, M. M.; Plaza, P.; Meyer, Y. H.; Badaoui, F.; Bourson, J.; Lefebvre, J. P.; Valeur, B. *J. Phys. Chem.* **1996**, *100*, 6879.
- (27) (a) Rodríguez, L.; Alves, S.; Lima, J. C.; Parola, A. J.; Pina, F.; Soriano, C.; Albelda, T.; García-España, E. *J. Photochem. Photobiol. A* **2003**, *159*, 253. (b) Ishikawa, J.; Sakamoto, H.; Nakao, S.; Wada, H. *J. Org. Chem.* **1999**, *64*, 1913. (c) Mori, Y.; Maeda, K. *Bull. Chem. Soc. Jpn.* **1997**, *70*, 869.
- (28) Rettig, W. P.; Maus, M. In *Conformational Changes Accompanying Intramolecular Excited-State Electron Transfer*; Waluk, J., Ed.; Wiley-VCH: Weinheim, Germany, 2000.
- (29) (a) Daub, J.; Engl, R.; Kurzawa, J.; Miller, S. E.; Schneider, S.; Stockmann, A.; Wasielewski, M. R. *J. Phys. Chem. A* **2001**, *105*, 5655. (b) McFarland, S. A.; Finney, N. S. *J. Am. Chem. Soc.* **2001**, *123*, 1260.
- (30) Rurack, K.; Bricks, J. L.; Schulz, B.; Maus, M.; Reck, G.; Resch-Genger, U. *J. Phys. Chem. A* **2000**, *104*, 6171.
- (31) Saha, S.; Samanta, A. *J. Phys. Chem. A* **2002**, *106*, 4763.
- (32) (a) de Silva, A. P.; Gunaratne, H. Q. N.; Habib-Jiwan, J.; McCoy, C. P.; Rice, T. E.; Soumillion, J. *Angew. Chem., Int. Ed. Engl.* **1995**, *34*, 1728. (b) Yorozu, T.; Hayashi, K.; Irie, M. *J. Am. Chem. Soc.* **1981**, *103*, 5480. (c) He, T.; Xu, T.; Zhao, Y.; Chen, C. *J. Chem. Soc., Perkin Trans. 2* **1999**, 545.
- (33) Huston, M. E.; Haider, K. W.; Czarnik, A. W. *J. Am. Chem. Soc.* **1988**, *110*, 4460.
- (34) Fahrni, C. J.; O'Halloran, T. V. *J. Am. Chem. Soc.* **1999**, *121*, 11448.
- (35) Kollmannsberger, M.; Rurack, K.; Genger-Resch, U.; Daub, J. *J. Phys. Chem. A* **1998**, *102*, 10211.
- (36) Fahrni, C. J.; Yang, L.; VanDerveer, D. G. *J. Am. Chem. Soc.* **2003**, *125*, 3799.
- (37) Kavarnos, G. J.; Turro, N. J. *Chem. Rev.* **1986**, *86*, 401.
- (38) Hancock, R. D.; Martell, A. E. *Chem. Rev.* **1989**, *89*, 1875.